ktu
1922

Kaunas University of Technology

Faculty of Mechanical Engineering and Design

Stress analysis and fatigue assessment of surge tank welded joints

Master's Final Degree Project

Abdulkhan Thorappa

Project author

dr. Evaldas Narvydas

Supervisor

Kaunas, 2020

Kaunas University of Technology

Faculty of Mechanical Engineering and Design

Stress analysis and fatigue assessment of surge tank welded joints

Master's Final Degree Project

Mechanical Engineering (code 6211EX009)

Abdulkhan Thorappa

Project author

dr. Evaldas Narvydas

Supervisor

Reviewer

Prof. Dr. Vytautas Grigas

Kaunas, 2020

Kaunas University of Technology

Faculty of Mechanical Engineering and Design

Abdulkhan Thorappa

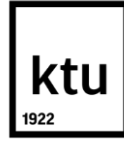# Stress analysis and fatigue assessment of surge tank welded joints

Declaration of Academic Integrity

Kaunas University of Technology

Faculty of Mechanical Engineering and Design

Study programme: MECHANICAL ENGINERING 6211EX009

Task Assignment for Final Degree Project of Bachelor Studies

Student – Abdulkhan Thorappa

1. Title of the Project –

Stress analysis and fatigue assessment of surge tank welded joints.

(In English)

Kompensacinės talpyklos suvirintų jungčių įtempių tyrimas ir patvarumo įvertinimas

(In Lithuaniain)

2. Aim and Tasks of the Project –

Aim- To design and analyse the surge tank welded structure and compare the model with different fatigue assessment techniques using local approaches.

Tasks

1. To analyse the publications and design codes for modelling of the surge tank and study the types of welded joints in the model.
2. To identify a model reduction technique in finite element analysis to reduce a complex structure for detailed analysis and fatigue assessment methods based on local approaches and validate the reliability of the model reduction technique.
3. Based on the model reduction technique, compare different fatigue assessment methods, and evaluate each method's effectiveness.

4. Initial Data –

Construction drawing of surge tank welded structure, which is operating with an internal pressure of 0.345 MPa.

5. Main Requirements and Conditions –

Should obtain the reliability of the model, and fatigue damage minimum as possible.

Project author

Abdulkhan Thorappa

(Name Surname)   *(signature)*   *(date)*

Supervisor

dr. Evaldas Narvydas

(Name Surname)   *(signature)*   *(date)*

Programme Director of the Study field

Assoc. Prof. Kęstutis Pilkauskas

(Name Surname)   *(signature)*   *(date)*

Summary

Stress distribution and fatigue analysis of complex welded structures are time-consuming and complicated procedures. Fatigue experiments of these complex structures might be expensive or even not possible. So, using the finite element analysis technique, stress information can be collected at a critical region of the complex models which includes steel bridges, pressure vessels, tanks, marine, and offshore structures. The structural stress of the model might vary with a sudden change in the model's shape, which might be at fillets, chamfers, and weld joints. The probability of failure occurs at the weld joints is higher, especially at the weld toe region. The structural stresses at the weld joint can predict the fatigue life of the entire model. The complex models might have hundreds and thousands of welded joints, thus, fatigue calculation with finite element analysis is the only solution to calculate the life of the entire model.

Fatigue analysis of welded joints required complete information about the critical region of the structure. The fatigue life depends upon the stress distribution and stress concentration factors at the welded joint which can determine using special approaches in the finite element analysis. One of the fundamental goals of fatigue design is to extrapolate structural stresses at the weld toe region without a weld notch effect, which is possible with the help of finite element analysis. It might capture membrane and bending structural stresses of the weldments.

This paper shows the design of a surge tank with the analysis of publications and design codes, and sub-modelling techniques in finite element analysis, which is a model reduction technique that allowed to concentrate on a critical region of the structure. The reliability of the model reduction technique is verified with deformation graphs at different notch radius, through-thickness, and along the surface of the model. Based on the model reduction technique, different fatigue assessment methods are compared using local approaches and studied recent development approaches to find the effectiveness of each fatigue assessment method.

Santrauka

Sudėtingų suvirintų konstrukcijų įtampių paskirstymo ir nuovargio analizė reikalauja daug laiko ir yra sudėtinga. Šių sudėtingų konstrukcijų nuovargio tyrimo eksperimentai gali būti brangūs ar net neįmanomi. Naudojant baigtinių elementų metodą informacija apie įtempius kritinėse zonose gali būti randama sudėtingose konstrukcijose, tokiose kaip plieniniai tiltai, slėginiai indai, rezervuarai, pakrantėse ir atviroje jūroje esančios konstrukcijos. Modelio konstrukcinis įtempis gali staigiai kisti, keičiantis modelio formai ties įvairiais briaunų suapvalinimais, nuožulomis ir suvirinimo siūlėmis. Tikimybė, kad konstrukcijos pažeidimas įvyks ties suvirinimo siūlėmis yra aukšta lyginant su kitomis zonomis. Suvirinimo jungties konstrukciniai įtempiai gali nulemti visos konstrukcijos tarnavimo laiką. Sudėtingose konstrukcijose gali būti šimtai ir tūkstančiai suvirintų jungčių, todėl nuovargio skaičiavimas pasitelkiant baigtinių elementų analizę yra vienintelis sprendimas visos konstrukcijos gyvavimo laikui apskaičiuoti.

Suvirintųjų jungčių nuovargio analizei atlikti reikėjo išsamios informacijos apie kritines konstrukcijos zonas. Konstrukcijos ilgaamžiškumas priklauso nuo įtempių pasiskirstymo ir suvirintos jungties įtempių koncentracijos veiksnių, kuriuos galima nustatyti naudojant specialius metodus baigtinių elementų analizėje. Vienas pagrindinių nuovargio prognozavimo būdų yra ekstrapoliuoti konstrukcijos įtempius per suvirinimo siūlės plotį neatsižvelgiant į įtempių koncentracijos efektą, o tai yra įmanoma atliekant baigtinių elementų analizę. Tokiu būdu galima išskirti suvirinimo vietos membraninius ir lenkimo konstrukcinius įtempius.

Šiame darbe išanalizuota kompensacinės talpyklos konstrukcija ir mokslinės publikacijos bei projektavimo standartai susiję panašių talpyklų projektavimu. Darbe išnagrinėti submodelių taikymo būdai baigtinių elementų analizėje, tai yra modelio redukcijos technika, leidusi sutelkti dėmesį į kritinę konstrukcijos dalį. Modelio redukcijos metodo patikimumas patikrintas deformacijų grafikais esant skirtingiems įpjovos spinduliams per sienelės storį ir išilgai modelio paviršiaus. Remiantis modelio redukcijos būdu lyginami skirtingi nuovargio įvertinimo metodai naudojant lokalios srities metodus ir naujausius pasiekimus šioje srityje siekiant nustatyti kiekvieno nuovargio įvertinimo metodo efektyvumą.

Table of contents

List of figures

List of tables

List of abbreviations and terms

Abbreviations:

ASME- American Society of Mechanical Engineers

ASTM- American society for testing material

IIW- International Institute of Welding

EN 13445- Euro standard of pressure vessel

FEA- Finite Element analysis

BS 5500- British standard for unfired, fusion welded pressure vessel

DNV- Standards for ships and offshore structures

UG- ASME parts for methods of construction and all materials

PWHT- Post weld heat treatment

PFHT- Post forming heat treatable

NDT-Non-destructive testing

RT - Radiographic Testing

UT -Ultrasonic Testing

MT- Magnetic Particle Testing

PT- Liquid Penetrant Testing

MAWP - Maximum allowable working pressure

Introduction

Fatigue failure is one of the main structural failures occurred in complex welded structures. These structures would become more vulnerable during their lifetime because of hazardous environmental conditions and ageing. Fatigue analysis of the complex welded structures would be an expensive, time consuming, and complicated procedure, which is possible with detailed information on stress distribution in a critical region. A complete stress information and stress distribution at the critical region in complex welded structures could be collected with the help of finite element analysis techniques. One of the fundamental goals of fatigue design in FEA is to extract structural stresses from the domain without the effect of weld toe notch stresses, in this way, fatigue assessment is possible with FEA.

The study aims to design and analyse the surge tank welded structure and compare the model with different fatigue assessment techniques using local approaches. The research raises the following tasks: -

a) To analyse the publications and design codes for modelling of the surge tank and study the types of welded joints in the model.

b) To identify a model reduction technique in finite element analysis to reduce the complexity of the structure for detailed analysis and fatigue assessment methods based on local approaches. Subsequently, justify the reliability of the model reduction technique.

c) Based on the model reduction technique, compare different fatigue assessment methods, and evaluate each method's effectiveness.

The design of the surge tank should satisfy quality requirements and meet the design standards. The method of extracting structural stress from the weld toe region of a surge tank is possible with special approaches in finite element analysis. Sub-modelling technique, mesh refinement techniques, and other modelling methods in FEA is applied to extract structural stress factors, membrane stresses, bending stresses, and non-linear peak stresses. Structural stresses obtained from finite element analysis used to determine the stress concentration factor and stress intensity factor at the weld toe region. The fatigue cracks might initiate with micro-cracking, and the stress information in this region usually finds the stress intensity and stress concentration factors.

The probability of fatigue crack initiation is higher at welding, especially at the weld toe and weld root region. The fatigue life of the welded structure is significantly lower than in the unwelded structure of the same material,[1] (See in **Fig. 1.**). Complex structures like steel bridges, nuclear power plants, pressure vessels, storage tanks, marine, and offshore structures, etc. would be installed with local structural FEA, and it might be hard to test the fatigue design of these models. Although, there are many techniques for measuring the quality of the weld including non-destructive testing methods, which only allowed users to detect the flaws inside the weld joint. Engineers should consider fatigue evaluation to determine the exact quality as well as the life of the model.

The execution of the FEA method into fatigue design using several approaches such as using the ASME approach, nominal stress approach, hot spot approach, effective notch stress approach, and some alternative method to find endurable structural stresses and strains. There might be some limitations or drawbacks for assessing the fatigue of a part using conventional methods. So, it is

observed that stress analysis and fatigue assessment of weld joints in surge tank would provide a more profound exploration of fatigue assessment technique, and it would increase the possibility of future study in microfracture of the material, and able to predict the life of the complex mechanical structures.
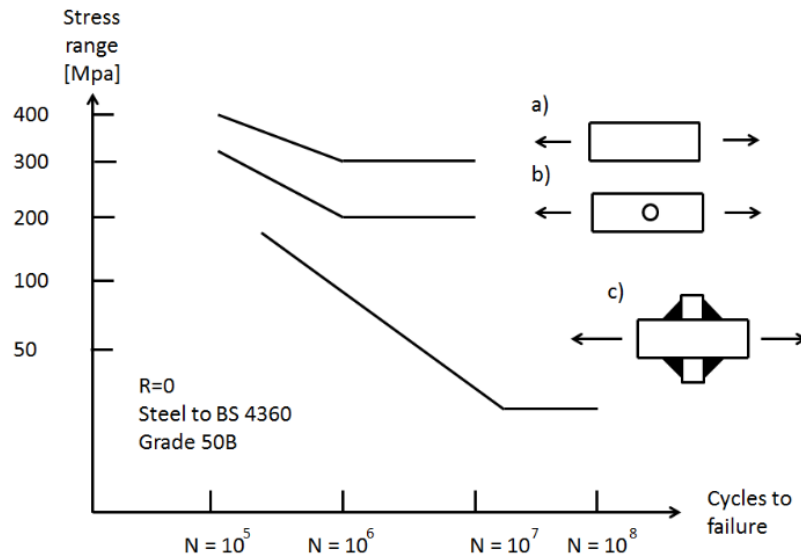
Fig. 1. Fatigue life comparison of the unwelded, notch and welded component

The model reduction technique in FEA is established to reduce the complexity of the model. Submodeling technique in ANSYS software is applied to study the area of interest in the surge tank welded joint. An article is submitted for publication in International Young Researchers Conference "Industrial Engineering 2020", which concluded the sub-modelling technique is an effective and more powerful method in FEA software for fatigue assessment study and verified the interpolation of nodal displacements from the global model to the sub-models are accurate.

1. Analysis of publications and design codes for modelling of welded joints in Surge tank

Surge vessels (surge tanks) would have a significant role in water treatment, which is used as a pressure neutralizer or a storage reservoir in many industries. The surge vessel acts as a water hammer in a pipe or storage tank at the downstream of closed end adequate, which absorbs sudden rises of pressure by oscillating the liquid inside the vessel. The Surge vessel is operating with compressed air or nitrogen, and the vessel water will go inside the vessel and let compress the gas until a balance occurs between the working liquid and the gas. Water will go inside the vessel with a small diameter, and several oscillations may occur before the static state is reached. Most surge tanks operate in a large reservoir, oil, and chemical industries, or a pipe that is placed in a vertical position to extend the water supply. It protects the damage of pipes, especially in weak joints like elbow, and small pipelines. When the load increases the surge tank allows water to move in from pipeline to the vessel, [2] and vice versa.

The surge tank is one of the most common types of pressure vessels with flanges and nozzles that are used in processing and manufacturing. The other common types of pressure vessels are storage tanks, process vessels, heat exchangers, etc. There are several classifications within the surge tank, and all have the same function but work differently. Gallery type, restricted orifice, differential surge tank, and simple surge tank are some of the examples. According to ASME design codes and standards, pressure vessels are containers that carry pressure either internally or externally. There are three types of pressure vessels according to their shape they are spherical, cylindrical, and conical which are usually constructed. Construction of pressure vessels according to design codes and standards is mandatory. The common types of pressure vessels are cylindrical with heads where the head shapes are usually hemispherical, elliptical, or tori-spherical dish end. The other shapes are employed and constructed but more expensive and complicated for construction. The spherical shape is more efficient for pressure vessels; however, it is more expensive, complicated for construction. Spherical, Cylindrical, and conical. The pressure vessel can further classify according to its dimensions and its position. If the ratio of wall thickness to the shell diameter t/d is less than 1/10 the vessel is said to be thin-walled pressure vessel, and the ratio of thickness to diameter t/d is more than 1/10, the vessel is a thick-walled pressure vessel. Pressure vessels may be the open or closed-end, longitudinal and hoop stresses are included in the closed type of pressure vessel, in open type only hoop stresses are included. A pressure vessel according to its position is horizontal, vertical, and inclined vessels.

1.1. Codes used for construction of Surge tank

The codes and standards are mandatory for the construction of pressure vessels, which might be different from countries around the world. One of the most common types followed by different regions and international companies is ASME Standards. shows [2] various sections of ASME design codes (See in **Fig. 2**), and ASME Section VIII Division1 and 2 generally used for the construction of pressure vessels, boilers, heat exchangers, and tanks.

ASME Boiler and pressure vessel code Sections

Section I	Rules for construction of Power boilers
Section II	Materials Part A - Ferrous material specification
	Part B - Non ferrous material specification Part C - Specifications for welding rods, electrodes, and Filler Metals Part D – Properties (Customary) Part D – Properties (Metric)
Section III	Rules for Construction f Nuclear Facility Components Subsection NCA – General Requirements for Division 1 and Division 2 Division 1 Subsection NB – Class 1 Components Subsection NC – Class 2 Components Subsection ND – Class 3 Components Subsection NE – Class MC Components Subsection NF – Supports Subsection NG – Core Supporrt structures Subsection NH – Class 1 Components in Elevated Temperature Service Appendices Division 2 — Code for Concrete Containments Division 3 — Containments for Transportation and Storage of Spent Nuclear Fuel and High Level Radioactive Material and Waste
Section IV	Rules for Construction of Heating Boilers
Section V	Nondestructive Examination
Section VI	Recommended Rules for the Care and Operation of Heating Boilers
Section VII	Recommended Guidelines for the Care of Power Boilers
Section VIII	Rules for Construction of Pressure Vessels Division 1 Division 2- Alternative Rules
	Division 3 - Alternative Rules for Construction of High Pressure Vessels
Section IX	Welding and Brazing Qualification
Section X	Fiber-Reinforced Plastic Pressure Vessels
Section XI	Rules for Inservice Inspection of Nuclear Power Plant Components
Section XII	Rules for Construction and Continued Service of Transport Tanks

Fig. 2. ASME Code details and Sections

Manufacturing and designing of pressure vessels should always follow codes and standards to make sure safe operation of equipment with appropriate design, materials, joining methods, and quality control of the equipment. Codes and standards used in many countries as described below and the subsection of ASME Section VIII Division 1 as shown in **Table 1.** [2].

USA - ASME section VIII Division- 1 &2

Britain - BS: 1500, EN13445, 806

Germany- DIN- EN13445, AD-MERKBLATT

India- UFPV 2825

China: GB-150

France: CODAP Division 1&2

Switzerland: ISO-TC-11

Table 1. Code formation of ASME Section VIII Division 1

Code formation of ASME SECTION VIII: Division 1		
Sub-Section A	General Requirement	Part UG- Construction methods and all materials
Sub-Section B	Fabrication Requirement	Part UW- Fabricated by welding, Part UF-Fabricated by forging, Part UB- fabricated for brazing
Sub-Section C	Vessel Material Requirement	Part UCS- Carbon and low alloy steels, PART UNF- Non-ferrous material-, Part UHA- High alloy steel, Part UCI- Cast Iron, Part UCL- Corrosion-resistant integral cladding or weld overlay cladding, Par UCD- cast ductile Iron, Part UHT- Ferritic steel with tensile properties enhanced by heat treatment, Part UIG- Impregnated graphite, Part ULW- layered construction, Part ULT- higher allowable stresses at low temperature, Part UHX- Shell and tube heat exchangers
Appendices	Requirement	Mandatory, Non-mandatory

1.2. Parts of the vessel

There are three main components in the pressure vessel [2], which is considered as basic they are the shell casing, some important attachments, and a base, and then finally the nozzle and a head.

1.2.1. Shell

The shell is the main component of every pressure vessel, constructed by plates rolled or welded together to form a structure. Weld joints in the shell would be either in the longitudinal or circumferential direction.

1.2.2. Head

The head closes the shell or end of the pressure vessels, which has mainly three different types as (See in **Fig. 3**) [2] a) Tori spherical head- the heads with a fixed radius and the transformation from the cylinder and dish is called the knuckle b) Hemispherical head- this is hemispherical equally across the surface c) Ellipsoidal head- this head is used in surge tank which is more economical and also called 2:1 elliptical head. Most of the head holds a curved configuration rather than flat, the curved configuration known as the knuckle region, which holds high pressure compared to other parts of the vessel.
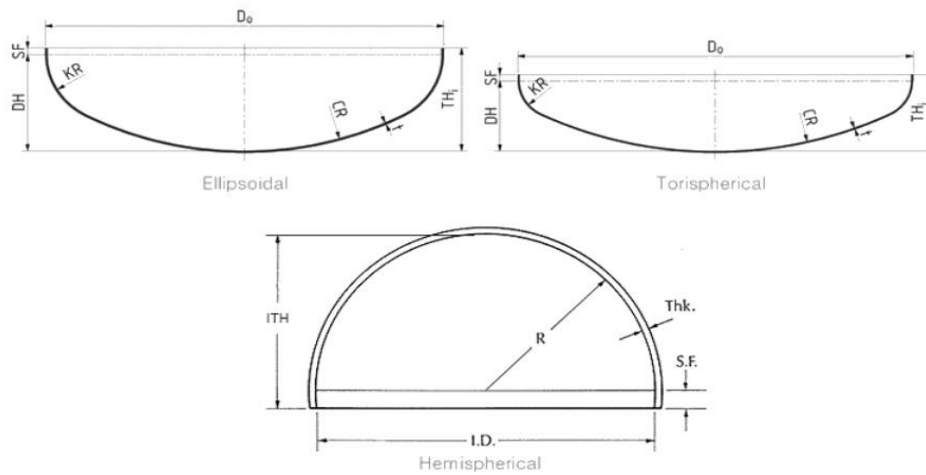
Fig. 3. Several types of shell heads

1.2.3. Supports

Supports carry all loads of the pressure vessel and consider it as a non-pressurized part fixed to the base by anchor bolt. Different types of supports depend upon pressure vessel configuration, operating temperate, location, and materials of the equipment. Four types of supports are commonly used, which are a) Leg support, b) Saddle support, c) Skirt Support, and d) racket support. More details available in ASME Section III, Subsection NF.

1.2.4. Nozzle

The nozzle is a cylindrical component that penetrates the pressure vessel either through shell or head, which can be either inlet or outlet nozzles. It should define as per the configuration of equipment. The nozzle gives the connection for instruments or maintenance of the equipment. Nozzle opening should be done according to ASME design codes section VIII division 1.

1.3. Type of weld joints in pressure vessel

Type of weld joints from design codes (See in **Fig. 4**) [2]. The categories established as follows
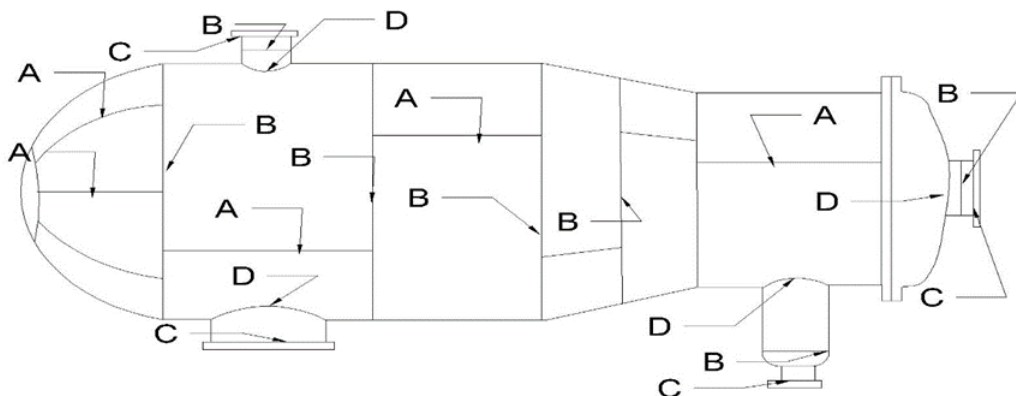
Fig. 4. Type of weld joints in Pressure vessel

18

1.3.1. Category A

Longitudinal and curved welded joints in the shell, change in diameter, and welded joints within the sphere are formed or flathead. These circumferential welded joints are connecting hemispherical head to the main shell.

1.3.2. Category B

Circumferential weld joints of the shell, nozzles, joints among the transition, communicating chambers and a cylinder. This is applicable to circumferential welded joints formed head other than hemispherical.

1.3.3. Category C

Welded joints in that are connecting flanges, nozzles, vessels, and any welded joint that are connecting one side plate to another side plate of the vessel., and weld joint for Van stone laps.

1.3.4. Category D
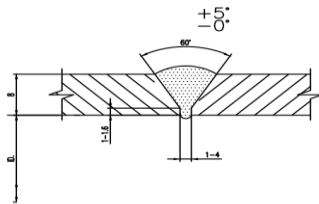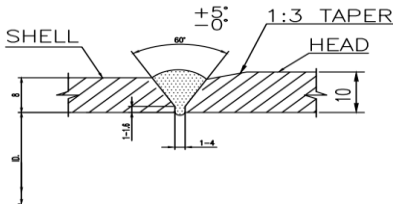
Weld joints are connecting Chambers or nozzles to the shell, head and flat side of the vessels, and nozzles connecting one side plate to another side plate of the vessel.
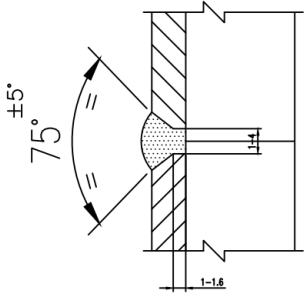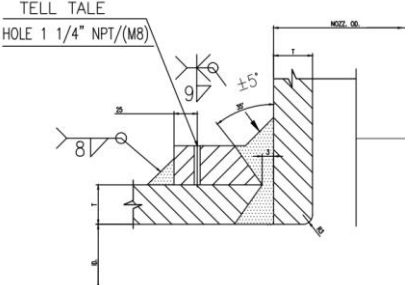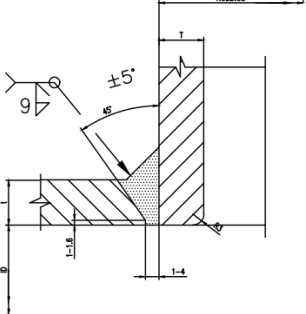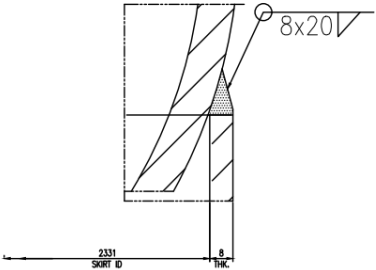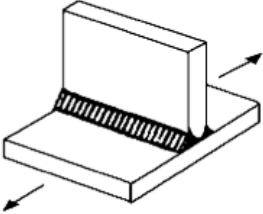
Welding material to produce equipment should allow ASME Section IX and the applicable qualified welding procedure specification. Welding material might be accepted or compliance with specification section II, part C ASME design codes and standards.

1.4. Weld joints in Surge tank

The main types of weld joints of the surge tank are shown in **Table 2**. However, some minor types of fillet joints are not shown, which should be considered with a minimum thickness of 6 mm fillet weld joint as per international design codes and standards.

Table 2. Type of Weld joints used in Surge Tank

Weld Joints	Weld Type	Model	Source
Long. Seam weld (LS1 and LS2) Shell to shell Joint	Butt Weld joint		ASME Section VIII Division 1
Circ. Seam weld (CS1 and CS2) Shell to shell Joint	Butt Weld joint		ASME Section VIII Division 1

Elbow/Flange to Nozzle	Butt Weld joint		ASME Section VIII Division 1
Nozzle neck to shell head/ Flange with Reinforcement pad	K butt weld joint		ASME Section VIII Division 1
Nozzle neck to shell head/ Flange	Butt weld joint with full penetration nozzle welded type		ASME Section VIII Division 1
Skirt to Dish End	Fillet Weld Joint		EN/DIN-13445-3
Base Skirt, Saddle support, and Lifting Lug	Fillet weld joint		EN/DIN 13445-3

1.5. Common types of welding

1.5.1. Gas Welding

Gas welding [2] is the process that used gas flames for melting two metals at the juncture. This is one of the oldest methods of joining metals. This method is comparatively easy and does not require an expert welder. Commonly for the aluminium-based material process, oxyhydrogen or oxyacetylene gas flames are used, which would reach a temperature of about 3100^0 Celsius.

1.5.2. Metal-Arc Welding

Metal-Arc Welding is also known as shielded metal arc welding or stick welding. It is made with standard dc equipment with opposite polarity (electrode-positive) and coated electrodes. Flux act as shielding from the outer atmosphere, both metal and workpiece melt to form a weld pool. For this type of Welding, worker skill is mandatory for high-quality welding.

1.5.3. Inert gas Metal arc welding

Both the consumable and non-consumable electrodes are used, which heats the workpiece, causing melt and set—this type of welding, either automatic or semi-automatic, which are advantageous particularly for the use of non-ferrous materials. The best results would be obtained with the use of filler materials.

1.5.4. Resistance welding

This welding can be done by joining of metals by applying pressure or resistance and passing current for a time of length, which forms a resistance weld joint. The main benefit of this type of joint is no extra materials require to create a bond to the subsection.

1.6. Pre and Post weld treatment method

If the size of the fillet weld or throat thickness not greater than 13 mm, available connections do not form ligaments to increase the shell and head thickness and preheat to a minimum temperature of 95^0C or 200^0F for materials P no. 1 (carbon low alloy steels) and the group no. 1,2, and 3, as per UCS 56-1.

Post weld treatment is a must when the welded joints over 38mm nominal thickness, and if welded joints over 32 mm nominal thickness and unless preheat are applied to a minimum temperature of 95^0 C during the welding process, as per UCS-56 PWHT is mandatory. Since specified minimal design melt temperature is not colder than -48^0 C, PWHT is not mandatory for this pressure vessel.

1.7. NDT requirements of surge tank

Non-destructive testing methods such as RT, UT, MT, and PT are applied to check the quality of the weld joint, which should follow ASME Section V Article 2. Longitudinal and circumferential weld joints of the vessel are butt weld joints which should have 100% radiography, not necessary for full radiography of other parts of the vessel unless the failure of spot radiography testing of a particular joint as the joint efficiency is RT-1 for the main welds of the surge tank.

2. Designing and calculation of Surge tank

Calculation material configuration would be necessary before the Finite element analysis. The surge tank has a capacity of 9320 Litres (3124 mm height x 2335 mm Internal diameter x 8 mm thickness).

2.1. Vessel design

Shell is the main component of the pressure vessel, [3] the thickness of the vessel is calculated based on the formulae from ASME Section VIII Division 1. The vessel might subject both internal and external pressure, and most of the cases, the internal pressure is higher than the external pressure. The minimum thickness or maximum allowable should be greater thickness and less pressure. The vessel would operate with an internal pressure of 0.345 MPa. The initial step of vessel design is to calculate the thickness of the pressure vessel, which includes the shell and the dish end. The formulae for calculating the thickness of the vessel as shown in **Table 3**, which would obtain from ASME Section VIII Division 1.

Table 3. Design calculation formulae for shell and head

Part	Thickness, t_p, (mm)	Pressure, P, (MPa)	Stress, S, (MPa)
Cylindrical shell	$\dfrac{Pr}{SE - 0 \cdot 6t}$	$\dfrac{SEt}{r + 0 \cdot 6t}$	$\dfrac{P(r + 0.6t)}{tE}$
2:1 elliptical head	$\dfrac{PD}{2SE - 0 \cdot 2P}$	$\dfrac{2SEt}{D + 0 \cdot 2t}$	$\dfrac{P(D + 0.2t)}{2tE}$

P-Internal working pressure of the shell

r-Internal radius of the shell

S- Maximum Allowable stress value

E-Joint efficiency of the shell joint, UW-12

t- thickness of the shell

The thickness of the shell calculated as 6.2 mm and for safety normally put 8 mm plate thickness, and for head 10 mm since the knuckle region possesses high-stress concentration compared to other parts of the vessel. [4][5]

The joint efficiency of the weld can be obtained from the standards. It defined as the reliability obtained from the weld joint after the welding procedure. The value always lower than 1, which is the other way to express the efficiency of the weld joint. Joint efficiency depends on the non-destructive testing method, and joint efficiency would decrease the allowable stresses of the material if it is far less than 1.

2.1.1. Design of nozzle and reinforcement pad

The nozzle's design starts with a procedure of removing material from the vessel, either shell or head. ASME codes simplify the opening of the nozzle with specific procedures. The calculations are made with respect to the metal cross-sectional area. There are seven types of nozzle opening according to ASME design codes and standards, they are according to the shape, opening size, design, and strength of finished opening, opening through welded joints, reducer section under internal and external pressure, and oblique conical shell sections under internal pressure.

Nozzle reinforcement is essential for nozzles under certain conditions according to ASME Section VIII Div1 as follows,

– The opening in the shells or heads, which is more than 89 mm or 3" nozzle welded with plate not less than 10 mm.
– In flat head openings
– Reducer section designed openings
– Large head openings
– Specific conditions of internal and external pressure.

The manhole is an unavoidable part of every vessel used for maintenance purposes. The manhole would be the highest nozzle in the vessel, as well as more chances of crack propagation at the manhole's weld joints of the manhole nozzle. The standard diameter of the manhole nozzle is about 508 mm and the reinforcement pad design (See in **Fig. 5** and **Fig. 6**) follows according to ASME design code Section VIII Div1 [2], UG-37. The reinforcement pad design purely depends upon the area outside the nozzle that should withstand the internal pressure of the vessel. Area of different sections of the nozzle A1, A2, A3, A5, A41, A42, A43, and weld load of reinforcement pad calculated from ASME section UG 37.1.
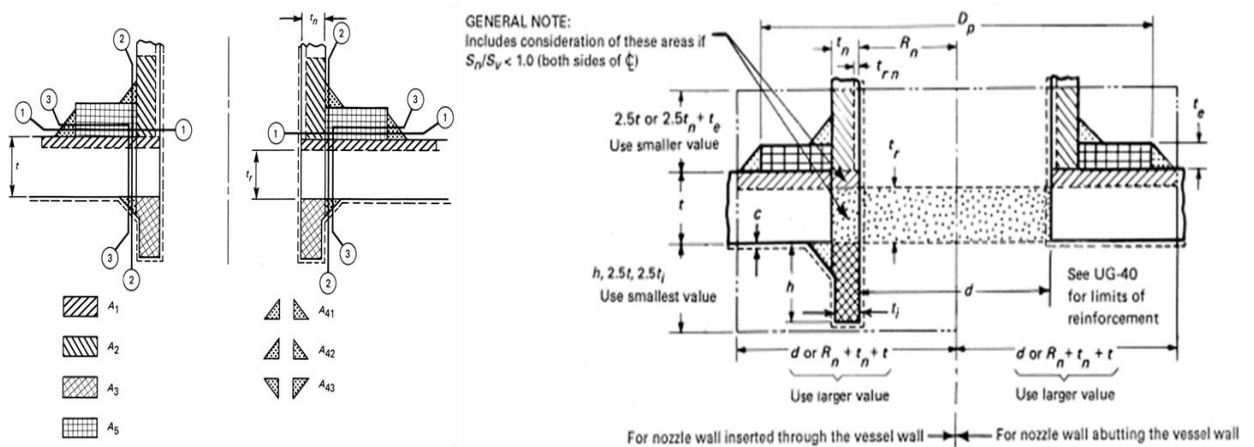
Fig. 5: Weld load path and area of cross section of reinforcement pad according to ASME code

Formulae for calculating of [2] areas $A_1, A_2, A_5 \ A_{41}, A_{42} \ A_{43}$ of reinforcement pad as shown **Table 4**.

Table 4: Formulae for calculating the area of reinforcement pad

Area Specification	Area Equations (mm2)

Area required A	$dt_r F + 2t_n t_r F(1 - F_{r1})$
Area available A_1	$d(E_1 t - Ft_r) - 2t_n(E_1 t - Ft_r)(1 - f_{r1})$
Area available in nozzle projecting outward A_2	$5(t_n - t_{rn})f_{r2}t$
Area available in inward nozzle A_3	$(D_p - d - 2t_n)t_e f_{r4}$

The reinforcement pad weld joints area calculated as per the formulae which are shown in **Fig. 6**
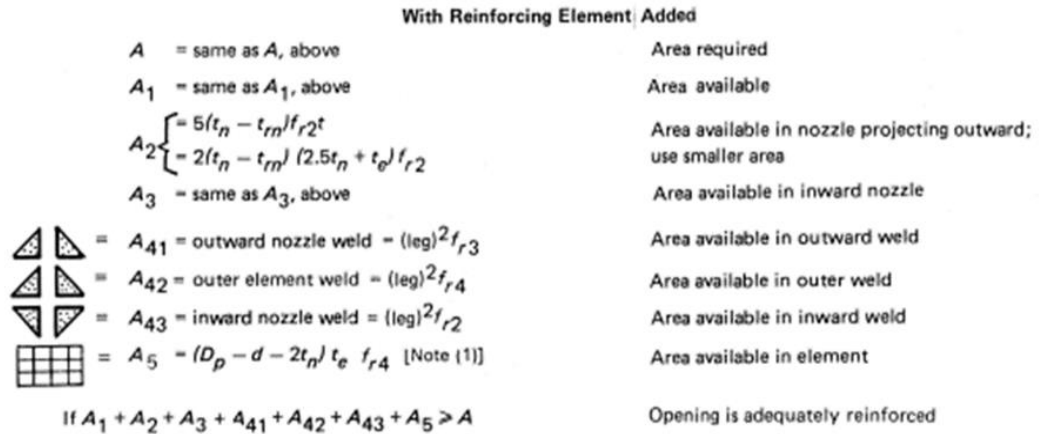
Fig. 6. Area calculation formulae of reinforcement weld joint

Weld load W, W_{1-1}, W_{2-2}, W_{3-3} as per UG-41[2] as equations for calculating as shown in **Table 5**, and the calculated values as shown in **Table 6.** Calculated reinforcement pad area and weld load

Table 5: Reinforcement pad weld load calculation formulae

Weld load Specification	Weld load calculation equations (N)
W	$[A - A_1 + 2t_n f_{r1}(E_1 t - Ft_r)]S_v$
W_{1-1}	$[A_2 + A_5 + A_{41} + A_{42}]S_v$
W_{2-2}	$[A_2 + A_3 + A_{41} + A_{43} + 2t_n t f_{r1}]S_v$
W_{3-3}	$[A_2 + A_3 + A_5 + A_{41} + A_{42} + A_{43} + 2t_n t f_{r1}]S_v$
W_{1-1}	$[A_2 + A_5 + A_{41} + A_{42}]S_v$

t_n- nominal thickness of the internal projection of nozzle wall

f_{r1}-Weld strength reduction factor which is not greater than one

S_v- Allowable stress value

t_r- required thickness of a seamless shell

F-1, correction factor

Table 6. Calculated reinforcement pad area and weld load

Area Specification	Area calculated (mm2)	Weld load Specification	Weld load calculated (N)
Area in shell A_1	1002.587	W	80,629.45
Area in Nozzle wall A_2	108.261	W_{11}	114,805.77
Area Required A	1567.413	W_{22}	30,668.89
Area in Nozzle wall $A_{41} + A_{42} + A_{43}$	87.750	W_{33}	121,705.06
Area in Element A_5	636.00	-	-
Total area available	1834.599	-	-

– Design of base and skirt support

The design of the skirt and base ring depends upon the weight of the vessel. The support is treated as a non-pressurized part as base skirt calculation of the vessel the same as per the shell design, and the thickness of the skirt plate calculated as 8 mm. The base ring estimated with a thickness of 20 mm, which is fixed to the ground by anchor bolt. The skirt outside diameter is 2347 mm and a thickness of 8 mm. The base ring is welded to the skirt in such a way that the skirt and base ring's internal diameter should match each other.

2.2. Material specification

The material for the construction of boiler and pressure vessels determined by ASME standard Section II [6], see in **Table 7** and ASTM standards confirm the strength of the material. ASTM SA 516 Gr70 material is the most popular material for the construction of pressure vessels, boilers, and tanks, which is primarily intended to use welded equipment. ASTM SA 516 material has four grades 55,60,65 and 70, which is based on the tensile strength of the material in the ksi unit. SA indicates the material, which is ferrous material and SB for non-ferrous material section II.

Table 7. Material Specification of vessel

Items	Material Specification	Allowable stress (MPa)	Reference of ASME Section II, Part D
Shell	SA-516M Gr. 485 (70)(N)	138	Table 1A, Page No.18, line No. 19

Head	SA-516M Gr. 485 (70)(N)	138	Table 1A, Page No.18, line No. 19
Reinforcement Pad	SA-516M Gr. 485 (70)(N)	138	Table 1A, Page No.18, line No. 19
Skirt Support	SA-516M Gr. 485 (70)(N)	138	Table 1A, Page No.18, line No. 19
Nozzle Flanges (WNRF)	SA-105M	138	Table 1A, Page No.18, line No. 5-
Nozzle Neck	SA-106 GR B	138	Table 1A, Page No.10, line No. 40-

The material specification of SA would find in ASME section II part D, and for SB material, it can be found in ASME section II part B. In the case of SA 516-70 carbon steel plates, the specified minimum ultimate stress or minimum tensile strength is 70 ksi or 485 MPa, and the minimum yield strength is 260 MPa. Shell, head, Skirt, and base ring are manufactured with SA 516 Gr 70 carbon steel plates, on the other hand, nozzle pipes are SA 106 Gr B which has a minimum yield strength of 240 MPa and Maximum tensile strength is 465 MPa, more detailed pipe schedules and charts could obtain from ASME B 36.1 and B 36.19. Most of the flanges are weld neck reinforcement flanges, which are welded with nozzle pipes. The flanges are SA 105M, a low-carbon steel alloy material with 250 MPa Yield strength, and 485 MPa minimum yield strength. More details of flange dimensions and specifications could obtain from ASME/ANSI B 16.5.

3. Finite element analysis and stress distributions of surge tank welded component

The stress concentration occurs when any discontinuities in the structural membrane and the stress are not uniformly distributed through the structure. The discontinuities may be a hole or notch, either in the edge or root of the notch. The peak stress is formed at the edge of the hole or notch root, which would be three times average stress. The notch effect in structure would considerably reduce the life of the structure. The stress concentration is developing due to the change of shape, not by reducing the cross-sectional area. Stress concentration does not affect the strength of the component under static loading conditions since the volume of highly stressed components is small compared to the material in nominal stress. Due to cyclic loading, high stresses repeatedly occur at this point, eventually crack initiation and failure occurs at this point. The stress concentration is more possible to happen at the toes of the weld joints. The sudden changes of material shape cause high stresses at the weld toe. There are several possible weld toe conditions, weld toe varies with toe angle, as undercut and convex profile have the most unfavourable conditions. The flaws at the weld toes such as slag inclusion, lack of fusion might increase the chances of failure.

3.1. Shell elements and solids in welded joints

The stress results from finite element analysis utilize shell elements deal using structural stress method and nodal forces. The stresses in the weld toe normally behave like multiaxial nature, which contains two normal stresses and one non-zero shear stress. The component which is perpendicular to the weld toe has a larger magnitude than in the x component. The more substantial magnitude component mostly accumulates fatigue damage in the weld toe region [7]. So, in practice, only the stress component vector considered across the thickness of the plate. The weld toe peak stresses (1) is the component membrane and bending stress. In structural structure without the effect of notch stress, nominal stresses act on other parts of the domain, which can be determined by simple tension and stress formulae.

$$\sigma_p = \sigma_m + \sigma_b = \frac{P}{t} + \frac{6 \cdot M}{t^2} \tag{1}$$

σ_p - peak stress

σ_m - membrane stress

σ_b - bending stress

In practice for surface stress extrapolation, relatively simple models and coarse mesh models are preferred for stress analysis. There are mainly two types of element models that explain the fatigue of weld toes that are shell and solid element models [8] (See in **Fig. 7**) as per ASME standards.
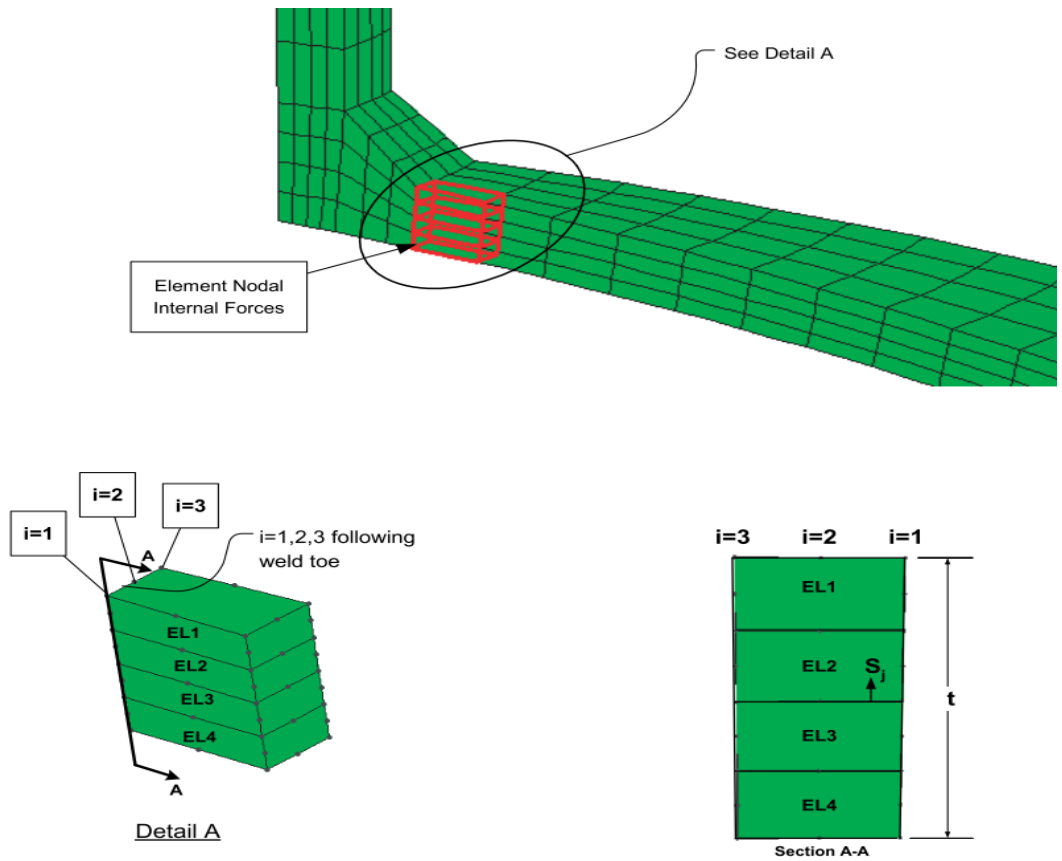
Fig. 7. Finite element model of Shell elements and Solids as per ASME section VIII Division 2

Elements are arranged in the middle plane of individual plates, and the weld is modelled in the standard or inclined shell elements, in case of eccentric shell weld arrangements.
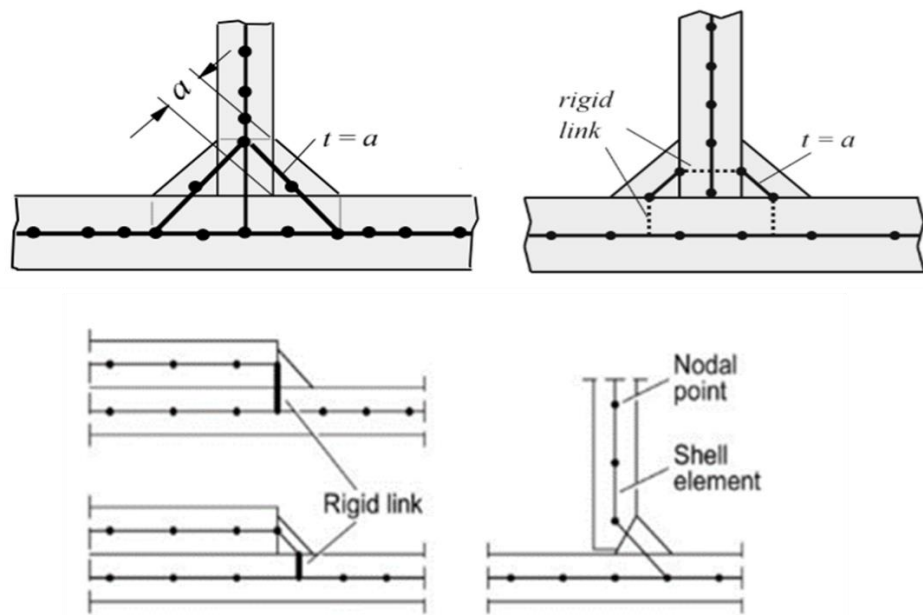
Fig. 8. T joint model with mid-side nodes and connection links

Shell element can be simulated in-plane stress gradients, as this element provides linear stress distribution over the thickness of the shell, which suppresses the notch stress due to weld toes.

In the case of measured surface stresses, the structural stresses are commonly extrapolated to the weld toe in case of measured surface stresses.

In solid elements, two models are possible; one element layer over the thickness and several arrangements of element layers. The single-layer 20 node element or hexahedral elements are recommended for solids and eight-node elements are recommended for shell elements. The thin shell elements naturally give linear stress distribution through the thickness of the shell, which excludes the notch stresses of the weld toe. The shell element models are significant sometimes to design the weld joint. In weld joint models, as shown in **Fig. 8** increase the cross-sectional cross might be a drawback of longitudinal joints. So, to solve that, add rigid links to the model in the midplane of the plates, which might be applicable to multi-point constraints in connection to the actual nodes.
`

3.2. Finite element analysis of Surge tank model

The Surge tank model is shown in **Fig. 9** and the finite element analysis of the global model as shown in **Fig. 10**, The surge tank operates with an inside pressure of 0.345 MPa, assuming negligible wind and snow loads, the vessel is fixed at the base ring. It allows deformation maximum at the manhole junction of the vessel, which is the largest opening and the largest nozzle of the vessel. The Surge tank has a total overall height of 3.1 m and 2.3 m internal diameter. Shell and head materials are carbon steel plates.
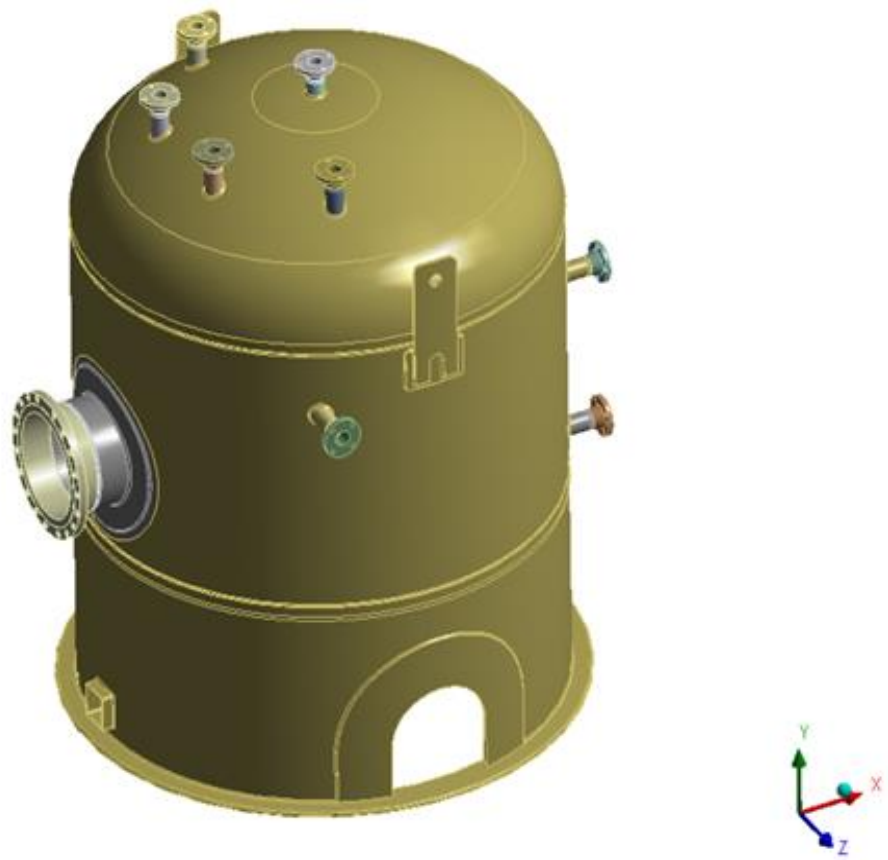
Fig. 9. Surge Tank Model
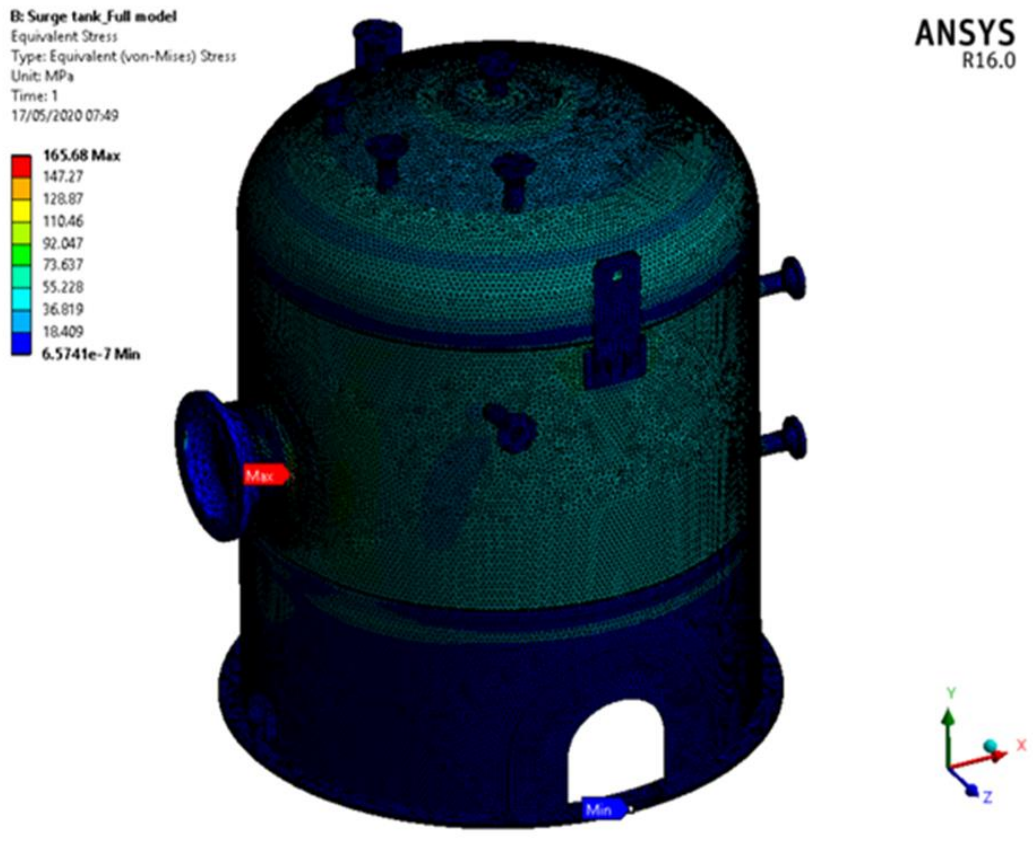
Fig. 10. Finite Element analysis of Surge tank model

SA 516 Gr (485) 70, SA - meaning ASME Boiler and Pressure Vessel material specification versus A, which is for ASTM material specification; 516 – number selected for carbon steel pressure vessel plate material. This material is most widely accepted for boilers, heat exchangers, pressure vessels, and storage tanks. It has a yield strength of 260 MPa and tensile strength of 485-650 MPa.

The surge tank with the capacity of 9320 litters, manufactured according to ASME Section VIII Division 1, and a more detailed analysis follows the ASME section VIII Division 2 standards. Plate thickness of shell and dish end was calculated as 8 mm; however, for an ellipsoidal head of the vessel, it would have a 10 mm nominal thickness for safety reasons since stress concentration would be more at the knuckle region of the head. Since this is a complex welded geometry, for detailed analysis, such a model requires either super elements or sub-modelling technique is required.

4. Model reduction Technique in finite element analysis

Submodeling technique is a model reduction technique in finite element analysis software that could concentrate on the local areal and reduce the complexity of the model. This technique is one of the most powerful methods in finite element analysis software. The cut boundary conditions of the sub-model often are determined by the interpolation of the calculated nodal displacements of the global model. The cut boundary is the smaller model or an area of interest that is cut from the global modal, and the cut boundary purely depends upon the user. The Sub-modelling approach is based on St. Venant's principle, which states that if an actual dispersal of forces is exchanged with a statically equivalent system, the distribution of stress and strain is different only near the areas of load application. This principle states that when the actual boundary conditions of the sub-model are replaced by the equivalent boundary conditions, there is no difference in the model response in the region, which is not close to the sub-model boundary. Although the sub-model size is determined by the user, the deformation should be checked with the global model so that the user can verify the model analysis. There are two types of basic sub-modelling techniques to define the boundary condition of sub-model: 1) displacement-based sub-modelling and 2) force-based sub-modelling. In displacement-based sub-modelling, the displacements of the global model are transferred to the faces of the sub-model, where it interacts with the global model, where it interacts with the global model. However, the major drawback of displacement-based sub-modelling is that the cut boundary displacements are valid only when the improvement of the sub-model does not change the stiffness comparing the initial global model. On the other hand, force-based sub-modelling reaction forces of the cut boundaries are transferred to the sub-model, which can be imported from the user-defined sources. The displacement-based sub-modelling are less sensitive to the mesh density of the global model [9].

The surge tank global model calculation might require more time for calculation, and the result could be inaccurate. Therefore, the sub-modelling technique in FEM supports to cut area of interest
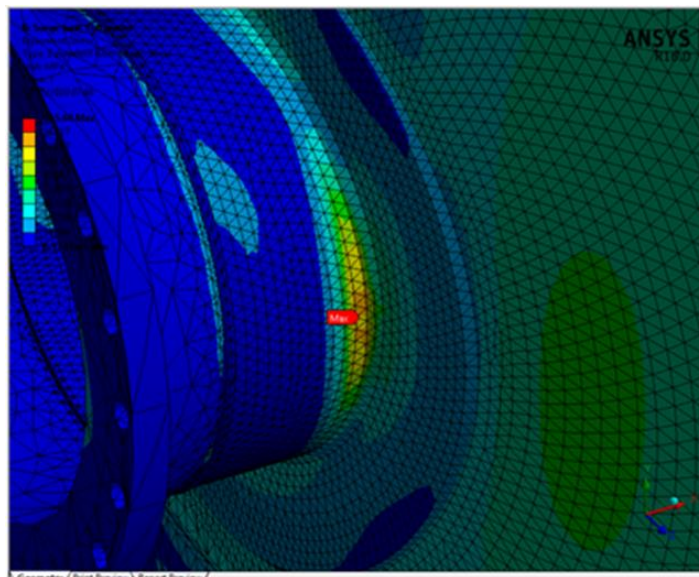
Fig. 11. Area of interest with high-stress concentration in Surge tank

from the global model to represent the domain for detail analysis (for construction purposes, fatigue assessments, weld analysis, fillets). Sub-models can be cut further into smaller sub-models to increase

the accuracy of the calculation. From the global surge tank model, the stress concertation higher at the manhole weld joint of the vessel which is shown in **Fig. 11**.

4.1.1. Software used for sub-modelling techniques

Sub-modelling technique supports finite element software such as ANSYS, ABAQUS, Nastran, and integrated CAD/CAE software (SOLIDWORKS Simulation). The ABAQUS software allows nodal based and surface-based sub-modelling. In nodal based sub-modelling, the global nodal results are interpolated onto the sub-model to obtain surface traction, supporting variety of element-type combinations and procedures. On the other hand, in Surface-based sub-modelling only available for solid to solid in sub modelling in static. Convergence difficulties may occur in surface-based sub modelling, so that inertia relief may be the solution [10] . Secondly, in ANSYS software, which is more advanced, less complicated, and allowing both nodal based and force-based sub-modelling for beam-to-solid, shell to solid (2D analysis to 3D analysis) and solid to solid (3D analysis to 3D analysis) sub-modelling system[11]. The sub-modelling technique could be successfully used for stress analysis and thermal, electromagnetic, and CFD analysis. Sub-modelling folder automatically created in ANSYS, which allows the definition of applied load, which would be either in displacement or body temperature, and this load must be applied to the cut boundaries of the sub-model, however, local body constraints should be defined in other parts of the sub-model. Finally, [12], in SOLIDWORKS, the sub-modelling technique is a fully automated, less complicated, and global model treated as a separate component or part, and it might have an incompatible mesh with other regions Sub-modelling techniques can be useful in different engineering fields such as structural mechanics [13] [14], electromagnetics [15], fracture mechanics [16][17], fatigue assessment [17].

4.1.2. Submodeling procedure

- The global model should be created and defined. Analysis should be done with appropriate meshing, and the area of interest should be defined.
- The sub-model size should be defined by the user based on the area of interest, which should be sliced from the global model for sub-modelling analysis.
- The sub-model is created by duplicating the global model and suppress all parts except the region of interest for detail analysis. The nodal displacement at the cut boundary must be derived from the global model.
- Mesh refinement and model correction can be done using the sub-model to increase the accuracy of the solution.
- Nodal displacement from the global model should be inserted to the sub-model's cut boundaries as the constraints and displacement should be inserted at this location, and the local boundary condition should be defined in the sub-model.
- Sub-model analysis should perform and can expect higher level accuracy in the solution or repeat sub-modelling technique in the local model at an infinite number of times until to get an accurate result.

4.1.3. Justification of Submodeling technique

Sub-modelling technique is accurate for a complete analysis of a critical joint of a global model. Sometimes, one sub-model might not be enough to get an accurate result, so the user can again divide the sub-model into an infinite number of parts as displacements should transfer from the global model to the sub-models. ANSYS software is more advanced for the sub-modelling technique. The folder

of a sub-model is created automatically immediately after connecting the global model's solution to the sub-model setup, which allows cut boundary constraints and displacement transfer from the global model to the sub-model. **Fig. 12** shows three different sub-models of a single global model, which is designed using ANSYS software.
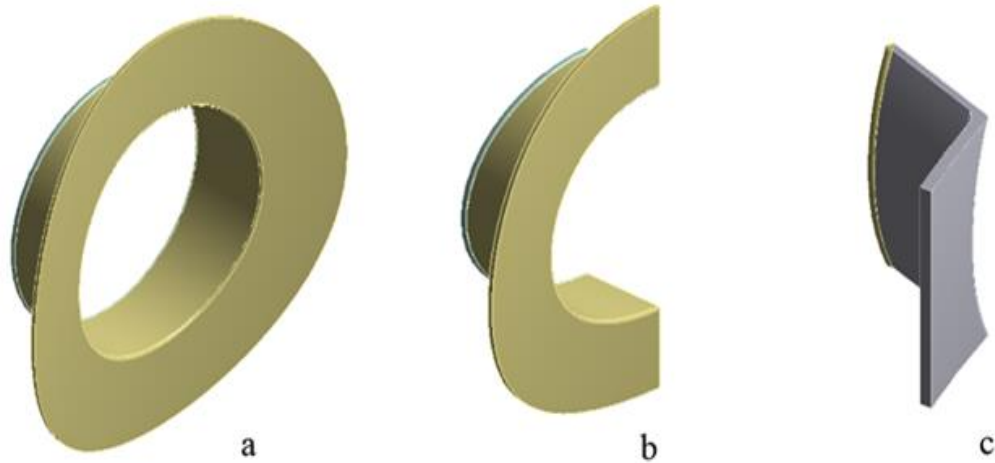
Fig. 12. Sub-models: a – sub-model 1 (an area of interest which is cut from global model), b – sub-model-2 (sub-model of sub-model-1) c – sub-model-3 (sub-model of the sub-model-2)

Stress distribution might vary from sub-model to sub-model. Stresses could be calculated by using the construction geometry path or surface, which would be created, based on a global coordinate system, as the global coordinate system should be the same for every sub-model. Therefore, the sub-models can be created only by duplicating the global model, and the sub-modelling technique might not work for other external domains. **Fig. 13** shows that the deformations are constant for every sub-model through the thickness of the shell (8 mm) it is calculated from ASME Section VIII Division 1, which confirms that the nodal displacement is transferred successfully from the global model to the sub-models.
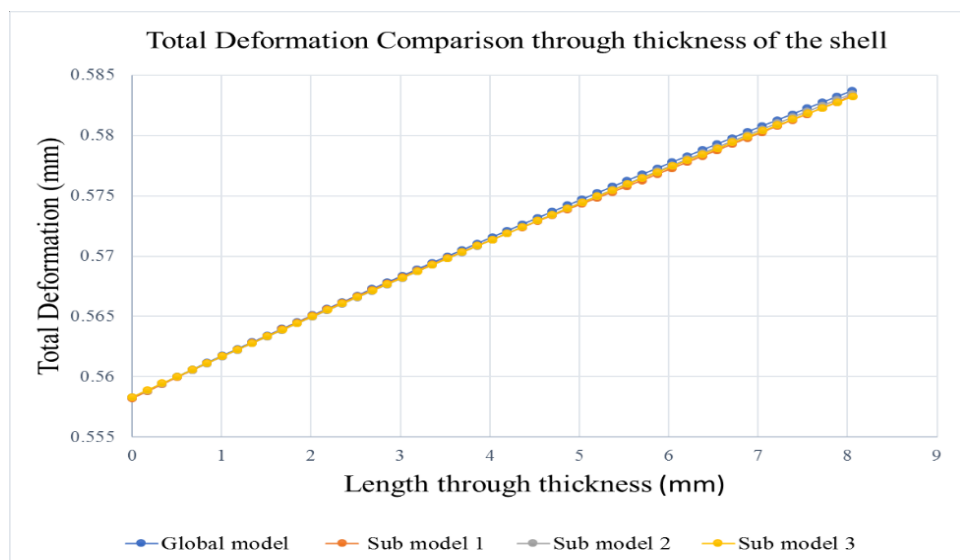
Fig. 13. Total deformation comparison of different sub-models through-thickness of the shell

One of the main goals of the sub-modelling technique is to achieve a fine mesh of the domain, which includes the region of interest. The comparison of course and fine mesh refinement is shown in **Fig. 14**, which shows the stress concentration is more at the weld toe region and the probability of crack initiation higher at this location.
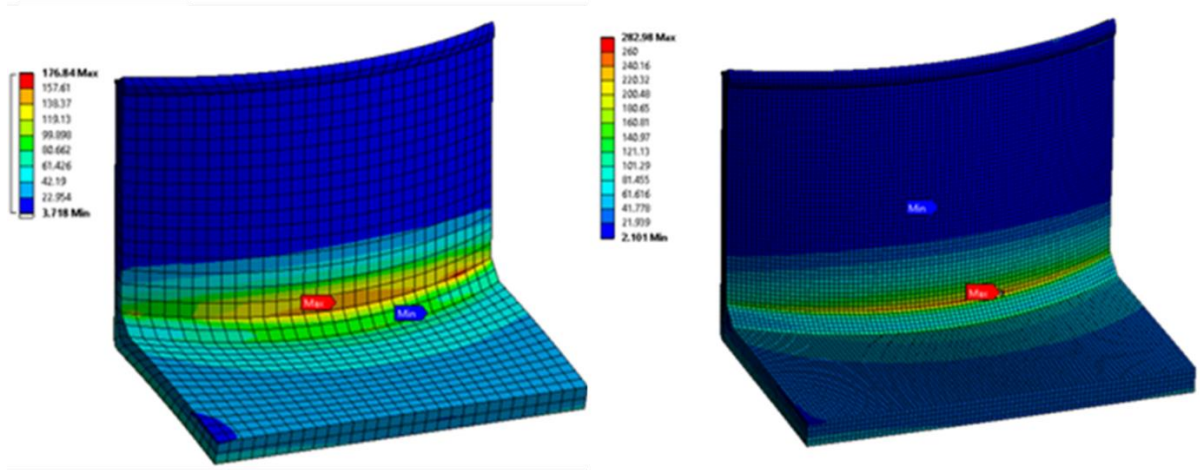
Fig. 14. Equivalent stress comparison for coarse and fine mesh of Sub-model 3

Equivalent stresses are increasing with mesh refinement, Coarse mesh gives a faster solution, but less accurate result; however, fine mesh gives a more precise result and need more time for calculation. Deformation would not affect the influence of mesh size, which remains the same along the weld toe region of the sub-model, which is shown in **Fig. 15**. The stress concentration could ne more at the weld toe region.
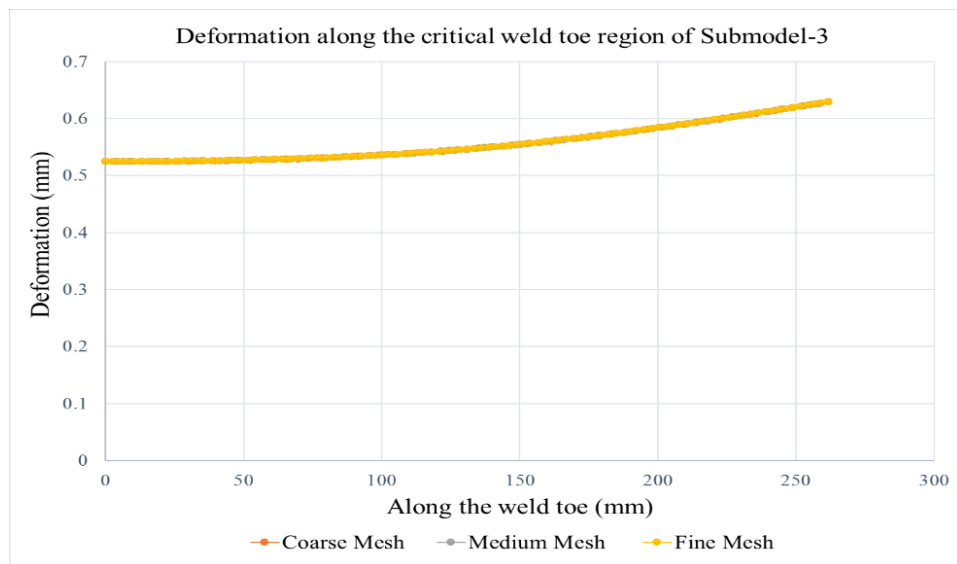
Fig. 15. Deformation along the critical weld toe regions of sub-models

By effective notch stress method, the stresses are calculated at the notches assumed to have linear elastic material characteristics. Interpreting variation of weld shape parameters, as well as non-linear material behaviour at the notch root, the actual weld outline based on international design codes and standards, are replaced with an effective one. For structural steels, notch effective root radius of r = 1 mm has been given consistent results. At weld toes, effective notch stress assumed as at least 1.6

34

times as structural hot spot stress. The effective notch stress method is limited to the thickness t greater than or equal to 5 mm. Equivalent stresses and stress concentration would increase with respect notch radius. However, the measured deformations along the weld toe region at different notch radius are constant, which is shown in **Fig. 16**, and the deformations are independent of notch radius. Therefore, the sub-modelling technique is valid for effective notch stress, crack prediction, and fracture mechanics calculations of complex welded structures.

	Notch radius (mm)		
	1	2	3
Min Deformation of 1mm, 0.5mm, 0.3mm notch radius	0.52374	0.52413	0.52429
Max Deformation of 1mm, 0.5mm,0.3mm notch radius	0.62996	0.62988	0.62986
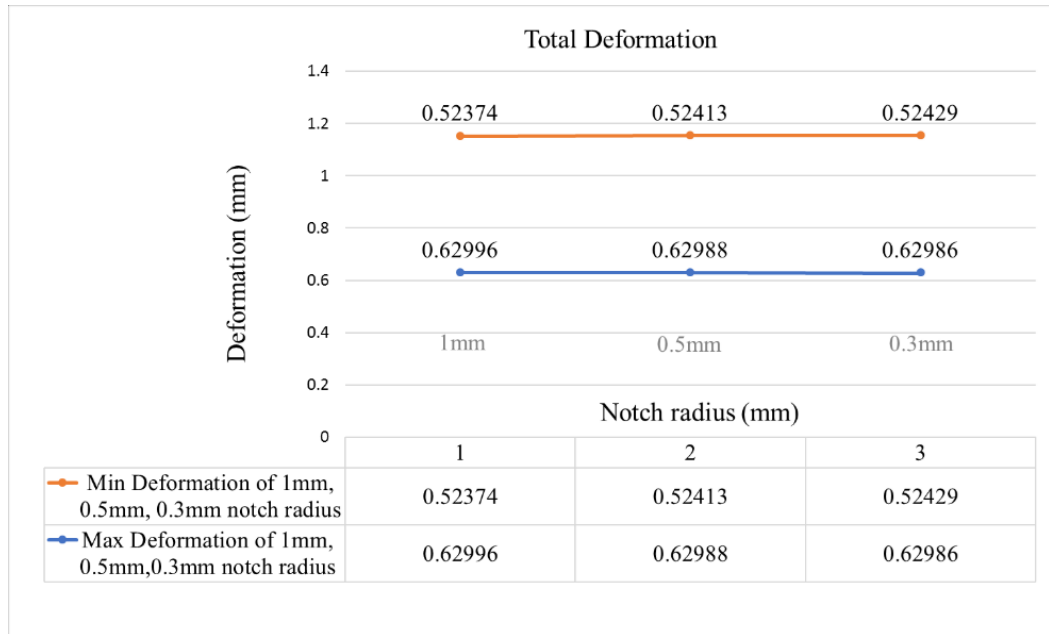
Fig. 16. Total deformation at different notch radius

5. Fatigue Assessment methods

The material fatigue is the phenomenon where structures failed due to cyclic loading, and the structural damage occurs when the stress range below the structural material strength. Most of the mechanical structures failed due to fatigue.

The process of fatigue failure under repeated loading is divided into three stages

- Due to many cycles the macroscopic crack growth from the microscopic level of damage.
- The macroscopic crack growth is obtained in each cycle until a critical length
- The breaking of cracked components due to peak load.

The last two stages usually considered as fracture mechanics topics, and fatigue term usually applies to the first stage. Most of the component experiencing microscopic crack before the component observe the microscopic crack or failure of the component.

The state of the material is defined under different variables such as stress, strain, and energy dissipation. The load cycle might vary in different or constant cycles see in **Fig. 17**. Variables to predict the material fatigue and the stress amplitude of one cycle to another cycle would be different. The stress might change between the maximum stress σ_{max} and a minimum stress of σ_{min}. In the fatigue cycle [18] the stress amplitude of σ_a.(3) with mean stress σ_m (2), the stress range of $\Delta\sigma$ (4) and the R value (5) is used to describe the stress cycle where the relation of different fatigue stress variables follows:

$$\sigma_m = \frac{\sigma_{max} + \sigma_{min}}{2} \tag{2}$$

$$\sigma_a = \frac{\sigma_{max} - \sigma_{min}}{2} \tag{3}$$

$$\Delta\sigma = \sigma_{max} - \sigma_{min} \tag{4}$$

$$R = \frac{\sigma_{min}}{\sigma_{max}} \tag{5}$$
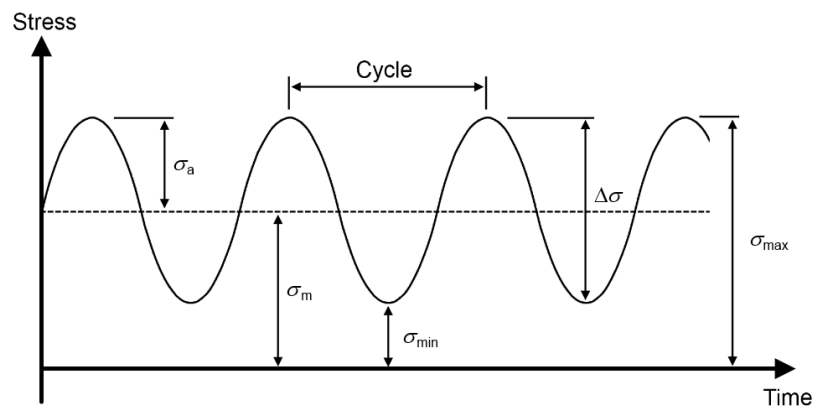
Fig. 17. Variables to predict the material fatigue

The stress amplitude is the most important parameter to determine the fatigue damage of the component, and the mean stress is taken when detailed analysis is required. The sensitivity of the material determines with mean tensile stress; on the other hand, the stress amplitude with mean compressive stress. The material behaviour due to fatigue purely depends on the nature of the external load, which might be random, periodic, or even consist of repeatable blocks.

Based on load cycle fatigue analysis, it is again classified as Low cycle fatigue (LCF), and High cycle fatigue (HCF), the limit between two cycles is 10^4. In the case of HCF, stresses would be low, and the stress-strain graph considered as elastic. The stress cycles would describe the life of the component using the S-N diagram. The detailed study of fatigue analysis developed in the 20th century. There is a limit in the S-N diagram, which is known as the endurance limit. And no fatigue damage of material is observed under this limit. There are different types of loading based on directions and locations, they are classified as uniaxial loading, biaxial loading, and multiaxial loading. Multiaxial loading means the stresses might change the directions and locations with respect to the external load, so that component might deform in different directions. So, it might be treated with the critical plane method, where many planes in space to predict the fatigue at the critical location of the component.

For fatigue analysis, the stress cycle is not possible to describe with a single stress amplitude, because each cycle is different. So, fatigue prediction is difficult compared to other analysis, in order to overcome this situation user should take the stress history and define a set of stress amplitude using Rainflow counting algorithm which might be used to define the stress amplitude with mean stresses. The linear damage rule found by Palmer-miners rule, which is one of the most popular rules to determine the fatigue at different stress levels. When structures have dynamic loading, which is under vibration, most likely to fail due to fatigue. The frequency assessment of fatigue could be done with the power spectral density method. In some material, the crack originates with microscopic defects, later it penetrates it into the material form a large defect. The defects at a critical location strongly influence the lifetime of the component, these stresses might decrease the lifetime of the component, which might occur under maximum principle stresses. So, probabilistic methods are used to predict the fatigue life of the component.

Fatigue tests can be done using Instron equipment to plot the hysteresis loop. Fatigue testing might be time-consuming, and the test runs in many cycles. The crystalline grains, the grain borders of the material influence the stress concentration. So, the large number of specimens should test and large scattering of load cycles, which could combine with available material data of similar type, to form a conclusion of reliability of the tested material. There are several types of finite element software accessible in the market for fatigue analysis design. ANSYS has one of the most cutting-edge software tools, NCODE extension for the detailed analysis of cyclic loading. [18]

5.1. Fatigue assessment procedures from ASME

The ASME design codes provide a certain evaluation technique [8] to determine fatigue failures. And the component should satisfy specific screening criteria. The fatigue curves based on a smooth bar test specimen and with weld joints. The smooth bar curves might be with or without weld joints. On the other hand, the weld joint curve does not exhibit endurance limit only applicable for welded joints. Three types of fatigue assessment procedures are available in ASME design standards-

- Elastic stress analysis and Equivalent stresses
- Elastic-plastic stress analysis and equivalent strains
- Elastic analysis and structural stress for weld joints.

Here, the surge tank only considering the Elastic analysis and equivalent stress, and elastic analysis and structural stress for welded joints.

5.1.1. Fatigue assessment-Elastic stress analysis and equivalent stress

In this method [8], an equivalent stress amplitude is applied to evaluate the fatigue in pressure vessels, which is obtained from linear elastic stress analysis. The important parameter to determine the fatigue is the total effective equivalent stress amplitude, which is half of the total equivalent stress range. The total effective equivalent stress range(6) is the combination of Local primary membrane equivalent stress (P_L), Primary bending equivalent stress P_b, Secondary equivalent stress (Q), and Peak equivalent stress(F), which is derived from the thickness of the section. The combination of all loads produced from specified operating pressures including mechanical loads, thermal loads, and loads due to other structural discontinuities. [19]

The effective total equivalent stress = $P_L + P_b + Q + F$ (6)

Assessment procedure

- To determine load history, which includes all operating loads applied to the component.
- To determine the individual stress-strain cycle of the material, using cycle counting method. To determine the stress tensor at the start and endpoints for the Kth cycle and evaluate the stresses for different structural loading conditions, including static loads and thermal loads. The effective equivalent stresses of static and thermal. (9), without the effect of thermal load (10), and the finite element software such as ANSYS can determine effective equivalent stresses of the component by finding von Mises stresses with static (7), and thermal load (8).

$$\Delta S_{pk} = \frac{1}{\sqrt{2}} \left[\begin{array}{c} (\Delta\sigma_{11k} - \Delta\sigma_{22k})^2 \\ +(\Delta\sigma_{11k} - \Delta\sigma_{33k})^2 + (\Delta\sigma_{22k} - \Delta\sigma_{33k})^2 + 6(\Delta\sigma_{12k}^2 + \Delta\sigma_{13k}^2 + \Delta\sigma_{23k}^2) \end{array} \right]^{0.5} \quad (7)$$

$$\Delta S_{LT,k} = \frac{1}{\sqrt{2}} \left[\begin{array}{c} (\Delta\sigma_1^{LT} - \Delta\sigma_2^{LT})^2 \\ +(\Delta\sigma_1^{LT} - \Delta\sigma_3^{LT})^2 + (\Delta\sigma_2^{LT} - \Delta\sigma_3^{LT})^2 \end{array} \right]^{0.5} \quad (8)$$

- To determine the effective equivalent stress amplitude in the Kth cycle, here the equation is used to calculate the value is

$$S_{alt,k} = \frac{K_f \cdot K_{e,k} \cdot (\Delta S_{pk} - \Delta S_{LT,k}) + K_{vk} \cdot \Delta S_{LT,k}}{2} \quad (9)$$

$$S_{alt,k} = \frac{K_f \cdot K_{e,k} \cdot (\Delta S_{pk})}{2} = 22.8 Ksi \quad (10)$$

$K_{e,k} = 1$ for $\Delta S_{n,k} <= S_{ps}$

$K_{e,k} = 1 + \frac{(1-n)}{n(m-1)} \left(\frac{\Delta s_{n,k}}{S_{ps}} - 1 \right)$ for $S_{ps} <= \Delta S_{pk} <= mS_{ps}$

$K_{e,k} = 1/n$ for $\Delta S_{n,k} >= S_{ps}$

Table 5.11
Weld Surface Fatigue-Strength-Reduction Factors

| Weld Condition | Surface Condition | Quality Levels (See Table 5.12) | | | | | | |
		1	2	3	4	5	6	7
Full penetration	Machined	1.0	1.5	1.5	2.0	2.5	3.0	4.0
	As-welded	1.2	1.6	1.7	2.0	2.5	3.0	4.0
Partial penetration	Final surface machined	NA	1.5	1.5	2.0	2.5	3.0	4.0
	Final surface as-welded	NA	1.6	1.7	2.0	2.5	3.0	4.0
	Root	NA	NA	NA	NA	NA	NA	4.0
Fillet	Toe machined	NA	NA	1.5	NA	2.5	3.0	4.0
	Toe as-welded	NA	NA	1.7	NA	2.5	3.0	4.0
	Root	NA	NA	NA	NA	NA	NA	4.0

Table 5.12
Weld Surface Fatigue-Strength-Reduction Factors

Fatigue-Strength-Reduction Factor	Quality Level	Definition
1.0	1	Machined or ground weld that receives a full volumetric examination, and a surface that receives MT/PT examination and a VT examination
1.2	1	As-welded weld that receives a full volumetric examination, and a surface that receives MT/PT and VT examination
1.5	2	Machined or ground weld that receives a partial volumetric examination, and a surface that receives MT/PT examination and VT examination
1.6	2	As-welded weld that receives a partial volumetric examination, and a surface that receives MT/PT and VT examination

Fig. 18. Weld Surface fatigue reduction factors

Table 5.13
Fatigue Penalty Factors for Fatigue Analysis

| Material | K_e [Note (1)] | | T_{max} [Note (2)] | |
	m	n	°C	°F
Low alloy steel	2.0	0.2	371	700
Martensitic stainless steel	2.0	0.2	371	700
Carbon steel	3.0	0.2	371	700
Austenitic stainless steel	1.7	0.3	427	800
Nickel-chromium-iron	1.7	0.3	427	800
Nickel-copper	1.7	0.3	427	800

NOTES:
(1) Fatigue penalty factor.
(2) The fatigue penalty factor should be used only if all of the following are satisfied:
   • The component is not subject to thermal ratcheting.
   • The maximum temperature in the cycle is within the value in the table for the material.

Fig. 19. Fatigue Penalty Factor Analysis table

The value of m - 2 and n - 0.2 for low alloy steels, see in **Fig. 19**.

K_f - the fatigue strength reduction factor,1 see in **Fig. 18**.

$K_{e,k}$ - the Fatigue penalty factor,1.3478.

K_{vk} - the Poisson correction factor=0.28. [8].

To estimate the permissible number of cycles (11) for the material carbon low alloy steels, 4xx series, which is calculated from a table of ASME design codes and standards and it is verified by given S-N curve of carbon low alloy steel material see in **Fig. 21**

$$N = 10^x \tag{11}$$

$$Y = log\left[28.3\, E3\left(\frac{Sa}{ET}\right)\right] \tag{12}$$

$$X = \frac{C_1 + C_3Y + C_5Y^2 + C_7Y^3 + C_9Y^4 + C_{11}Y^5}{1 + C_2Y + C_4Y^2 + C_6Y^3 + C_8Y^4 + C_{10}Y^5} \tag{13}$$

Sa - Computed stress amplitude

E_T - Modulus of Elasticity of the material

N - Number of allowable design cycle

C1, C2,..C10 - Coefficient of fatigue cure see in **Fig. 20**

Coefficients C_i	$48 \leq S_a < 214\,(MPa)$ $7 \leq S_a < 31\,(ksi)$	$214 \leq S_a \leq 3999\,(MPa)$ $31 \leq S_a \leq 580\,(ksi)$
1	2.254510E+00	7.999502E+00
2	-4.642236E-01	5.832491E-02
3	-8.312745E-01	1.500851E-01
4	8.634660E-02	1.273659E-04
5	2.020834E-01	-5.263661E-05
6	-6.940535E-03	0.0
7	-2.079726E-02	0.0
8	2.010235E-04	0.0
9	7.137717E-04	0.0
10	0.0	0.0
11	0.0	0.0
Note: $E_{FC} = 195E3\ MPa\ (28.3E3\ ksi)$		

Fig. 20. Coefficient of fatigue curve for carbon low alloy steel 4xx steel material

   – To determine the fatigue damage (14) for the Kth cycle, the far less fatigue damage value have more fatigue cycle than the value which is closest to or more than one.

$$D_f = \frac{n}{N} = \frac{1000}{1.202 \times 10^5} = 0.008 \tag{14}$$
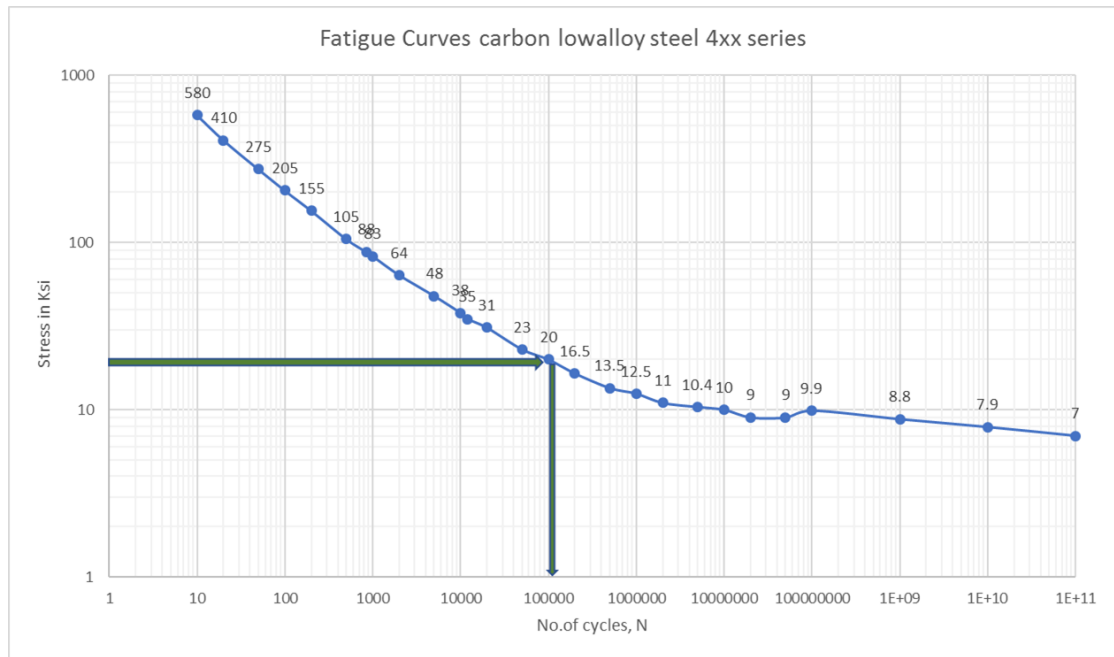
Fig. 21. The number of cycles verified with given fatigue curve data of carbon low alloy steel

− Repeat steps from step 3, to find the fatigue damages of various critical locations

5.1.2. Fatigue assessment of welds-Elastic analysis and structural stress

In this method, an equivalent stress range is applied to analyse the fatigue of a component from linear elastic stress analysis results. Here, the controlling parameter is the structural stress, which is a function of the membrane and bending normal to the hypothetical crack, as this method is suggested to the weld joint, which has not been machined to a smooth profile. The fatigue cracks usually located at the weld toe joint. The fatigue crack is along the weld toe through-thickness direction, and the structural stress expected to form a crack is correlated with material life data. Fatigue cracking at the fillet weld joint and more chances of occurring at the root and toe of the weld joint, both parts considered for fatigue assessment. Weld throat life is difficult to predict which is entirely depends upon the welder.

Assessment procedure

− To determine the load history of the material, which includes all operating loads of the component.
− For the position of the weld joint, which is subjected to fatigue evaluation, and analyse the stress-strain cycle using cycle counting method.
− Calculate the membrane and bending stress of the weld joint see in **Fig. 22** and **Fig. 23**, which is assumed to be normal to the hypothetical crack. Finite element software such as ANSYS, which allows to extract membrane and bending stress through-thickness.

Thickness Linearization:

For calculating the peak stresses at the weld toe, it is necessary to extract or calculate membrane (15) and bending stresses (16) at the critical location of the vessel or weld toe location. This can be calculated either through manual calculation or using finite element software such as ANSYS as see in **Fig. 24** and **Fig. 25.**
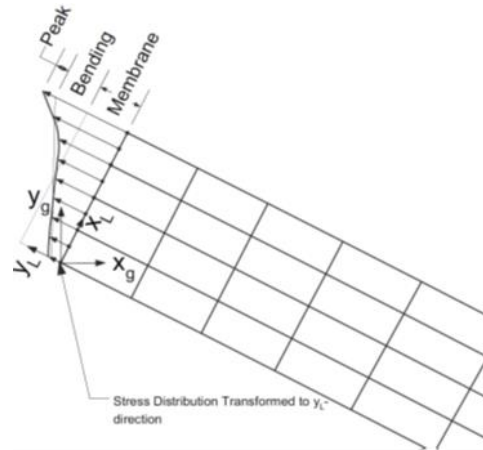
Fig. 22. Nodal forces at the elements
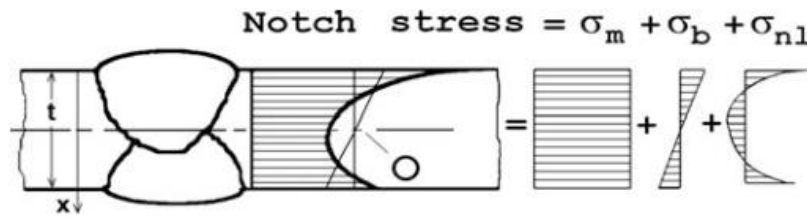
Fig. 23. Non- Linear distribution of stresses in shells and components

$$\sigma_m = \frac{1}{t} \int_{x=0}^{x=t} \sigma(x)\, dx \qquad \text{(Membrane stress)} \tag{15}$$

$$\sigma_b = \frac{6}{t^2} \int_{x=0}^{x=t} (\sigma(x) - \sigma_m).\left(\frac{t}{2} - x\right) dx \qquad \text{(Bending stress)} \tag{16}$$

$$\sigma_{nl} = \sigma(x) - \sigma_m - \left(1 - \frac{2x}{t}\right).\sigma_b \qquad \text{(peak non-linear stress)} \tag{17}$$
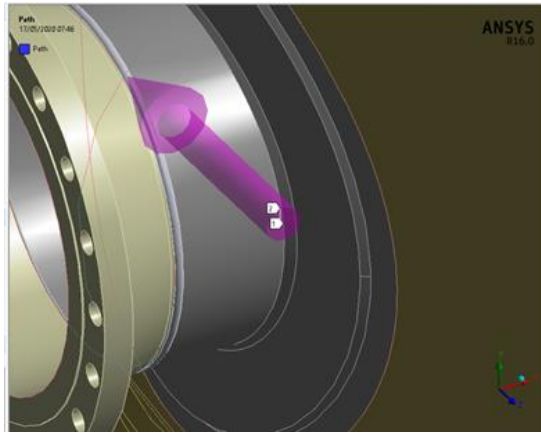
Fig. 24. Membrane and bending stress extraction procedure through-thickness of the shell
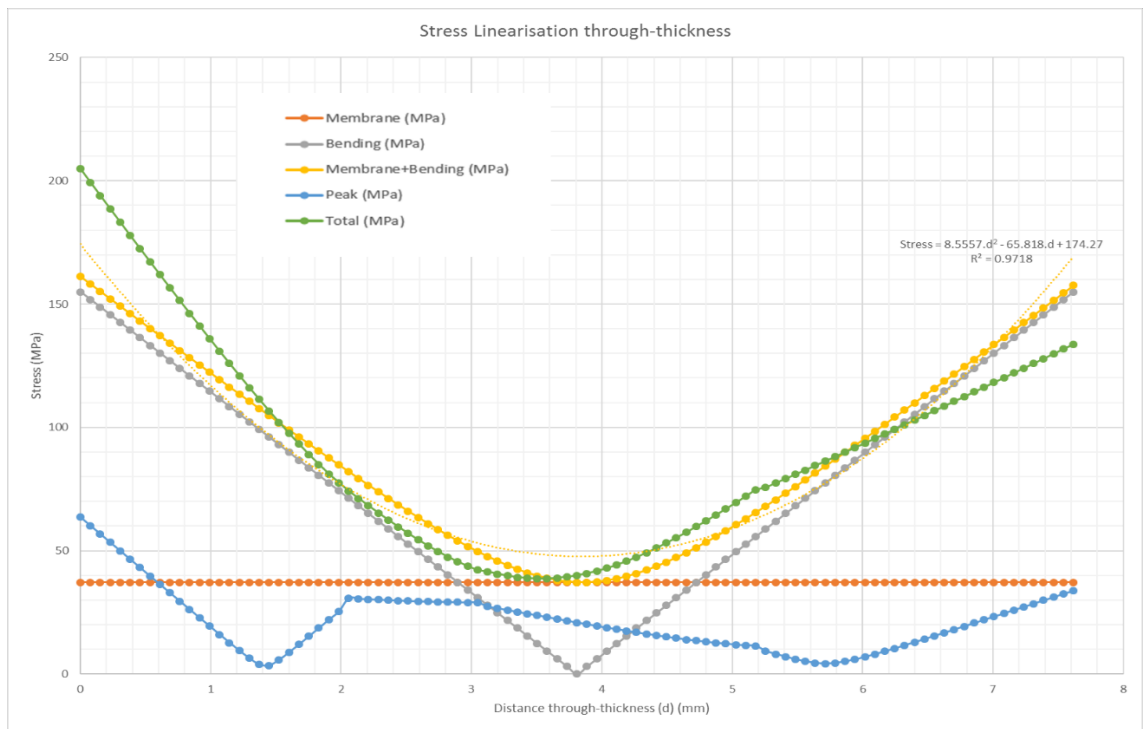
Fig. 25. Stress Linearization graph through-thickness of the shell

− To determine elastically calculated structural stress range in Kth cycle

To analyse elastically calculated structural stress $\Delta\sigma_k = 161\ MPa$ using elastically calculated structural strain $\Delta\varepsilon_k$. The non-linear structural stress is determined by Neubers Rule (20), and the hysteresis loop of the model, E_{ya} is the modulus of elasticity and ν is the Poisson's ratio and the equation as follows:

$$\Delta\sigma_k\ \Delta\varepsilon_k = \Delta\sigma^e\Delta\varepsilon^e \tag{18}$$

$$\Delta\varepsilon_k = \frac{\Delta\sigma_k}{E_{ya}} + 2\left(\frac{\Delta\sigma_k}{2kc_{ss}}\right)^{\frac{1}{n_{c_{ss}}}} \tag{19}$$

$$\Delta\sigma_k = \left(\frac{E_{ya,k}}{1-v^2}\right)\Delta\varepsilon_k \tag{20}$$

kc_{ss} and nc_{ss} are the material constant which can be obtained from hysteresis stress-strain curve the values of these are shown in **Fig. 26**.

<div align="center">

Table 3-D.2
Cyclic Stress–Strain Curve Data

</div>

Material Description	Temperature, °F	n_{css}	K_{css}, ksi
Carbon Steel (0.75 in. — base metal)	70	0.128	109.8
	390	0.134	105.6
	570	0.093	107.5
	750	0.109	96.6

<div align="center">

Fig. 26. Material constant from cyclic hysteresis stress-strain curve

</div>

- To calculate the equivalent structural stress parameter at the Kth cycle with stress range, which is obtained from the above equation, the equivalent structural parameter (21) is calculated using the formulae as follows

$$\Delta s_{ess,k} = \frac{\Delta\sigma_k}{t\,ess^{\left(\frac{2-mss}{2m_{ss}}\right)} I^{1/m_{ss}} f_{M,k}} \tag{21}$$

$m_{ss} = 3.6$

$t_{ess} =$ thickness effect 16mm (if the thickness of the plate is less than 16mm)

$$I^{1/m_{ss}} = \frac{1\cdot23 - 0\cdot364 R_{bk} - 0.17 R_{bk}^2}{1.007 - 0\cdot306 R_{bk} - 0.178 R_{bk}^2} \quad \text{(load type effect)} \tag{22}$$

$$R_{bk} = \frac{|\Delta\sigma_{b,k}|}{|\Delta\sigma_{m,k}| + |\Delta\sigma_{b,k}|} \tag{23}$$

(ratio of bending stress to the membrane plus bending stress for the Kth cycle)

To compute the permissible number of cycles N_k which is calculated (24) based on equivalent structural stress range K^{th} cycle, and values of coefficient of welded joint fatigue curve as shown in **Fig. 27**.

Table 3-F.2M
Coefficients for the Welded Joint Fatigue Curves

Statistical Basis	Ferritic and Stainless Steels		Aluminum	
	C	h	C	h
Mean Curve	19930.2	0.31950	3495.13	0.27712
Upper 68% Prediction Interval $(+1\sigma)$	23885.8	0.31950	4293.19	0.27712
Lower 68% Prediction Interval (-1σ)	16629.7	0.31950	2845.42	0.27712
Upper 95% Prediction Interval $(+2\sigma)$	28626.5	0.31950	5273.48	0.27712
Lower 95% Prediction Interval (-2σ)	13875.7	0.31950	2316.48	0.27712
Upper 99% Prediction Interval $(+3\sigma)$	34308.1	0.31950	6477.60	0.27712
Lower 99% Prediction Interval (-3σ)	11577.9	0.31950	1885.87	0.27712

GENERAL NOTE: In SI units, the equivalent structural stress range parameter, $\Delta S_{ess,k}$, in 3-F.2.2 and the structural stress effective thickness, t_{ess}, defined in 5.5.5 are in $MPa/(mm)^{(2-m_{ss})/2m_{ss}}$ and millimeters, respectively. The parameter m_{ss} is defined in 5.5.5.

Fig. 27. Coefficients for welded joint fatigue curves

Weld fatigue curve

$$N = \frac{f_1}{f_E}\left[\frac{f_{MT} \cdot C}{\Delta S_{ess,k}}\right]^{1/h} \tag{24}$$

f_E is the Environmental modification factor

f_1 are the fatigue improvement methods

For burr grinding following part 6

$$f_1 = 1 \cdot 0 + 2.5.(10)^q \tag{25}$$

For TIG dressing

$$f_1 = 1 \cdot 0 + 2.5.(10)^q \tag{26}$$

For hammer peening

$$f_1 = 1 \cdot 0 + 4.(10)^q \tag{27}$$

In the above equations, the parameter q is defined as follows:

$$q = -0.0016(\Delta S_{range}.C_{usm})^{1.6} \tag{28}$$

ΔS_{range} = equivalent structural stress range

$C_{usm} = 1$ in Mpa conversion factor

To evaluate the fatigue damage for the Kth cycle and the repetition of cycles n_k for the actual number of cycles is

$$D_{f,k} = \frac{n_k}{N_k} = \frac{1000}{1.29 \times 10^5} = 0.0077 \tag{29}$$

    − Repeat the steps for fatigue evaluation of the weld joint.

5.2. Fatigue assessment procedure from IIW, EN13445-3

5.2.1. Nominal Stress Method

The nominal stresses are the stress calculated the sectional area ignoring the stress raised by welded joint, but including the macro geometric shape of the component, [20] this stress allowed to evaluate fatigue analysis and service life of structural members with nominal stress amplitude compares with S-N curve (FAT 80) of nominal stress amplitude of the weld structures. The slope of the S-N curve approximately predicts the design life of the model see in **Fig. 28**. Nominal stress permissible number of cycles evaluated with FAT class 80. According to the relative form of Miner's rule, the nominal hypothesis is a simple hypothesis of damage formation.

The measurement of nominal stress (30) is done by placing strain gauges, which is placed outside the stress concentration of the welded joint. Finite element analysis would be used by using a probe tool when the structures are statically over-determined complex structures and macro-geometric discontinuities in the components.

$$\sigma_w = \frac{F}{A_\omega} = \frac{F}{a..l_\omega} \tag{30}$$

l_ω − weld length

a − throat thickness

σ_w − nominal Stress

ANSYS software calculates forces at nodes of solid elements and forces and moments at nodes of shell elements. Extracting these forces and moments and calculating the average nominal stress and stress in the nominal approach, nominal stress is calculated from ANSYS software, which is 157 MPa, and compare with FAT class 80.
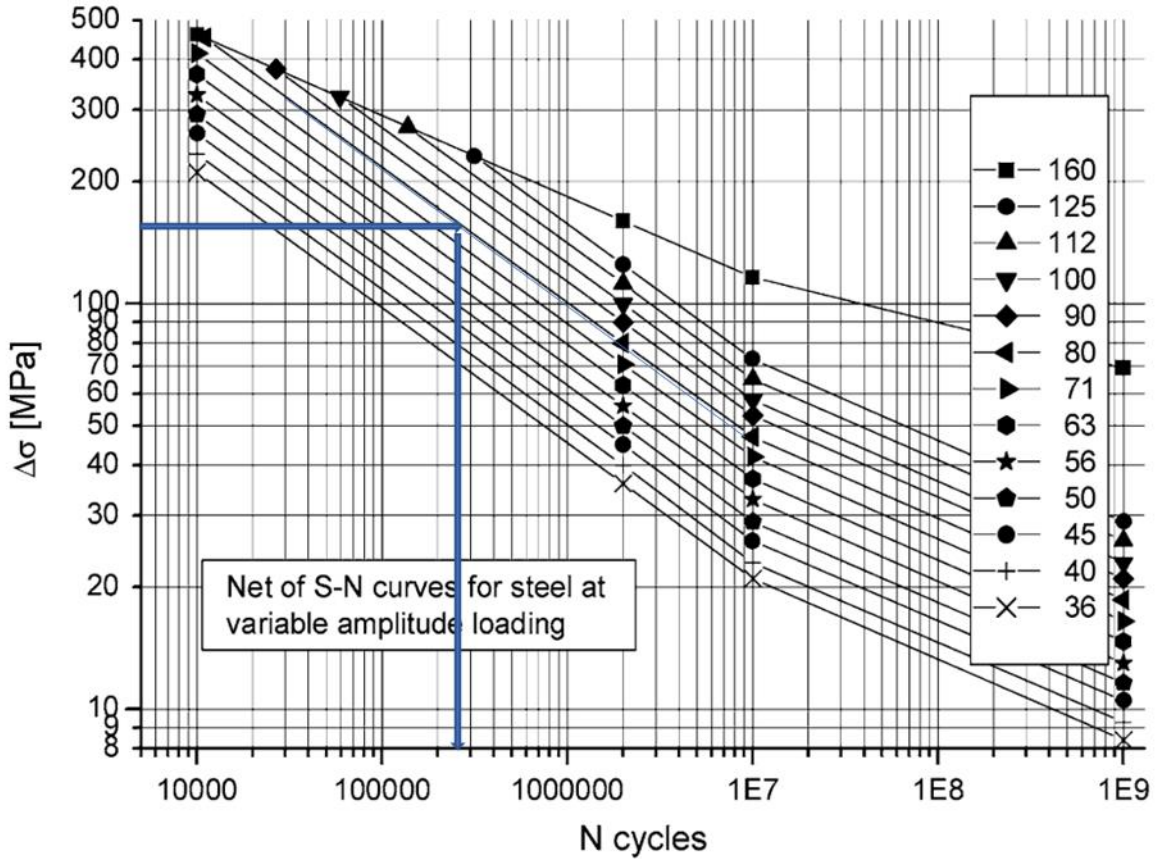
Fig. 28. Nominal stress permissible number of cycles evaluated with FAT class 80

The nominal stress approach (31) to steel and Aluminium is essential, and the formulae are reviewed, which can be explained in S-N curves linearized in logarithmic scales

$$\sigma_{nA} = \left(\frac{N_E}{N}\right)^{1/k} \sigma_{nAE} \tag{31}$$

σ_{nA} − nominal stress amplitude

σ_{nAE} − constant amplitude endurance limit

N_E -10^7 cycles for normal stresses and 10^8 cycles for shear stresses

N- is the endurable number of cycles

k - is the inverse slope of fatigue curve, for normal stresses, and shear stresses.

5.2.2. Hot Spot Stress Method

The structural hot spot method includes all stresses of a structure but excludes the stresses of the weld profile. The structural hot spot stress (SHS) can be calculated using a linear extrapolation method with two reference points, See in **Fig. 29.** Structural hot spot (SHS) definition so that nonlinear peak of the weld notch can be omitted. The SHS is clear for the plate, shell and tubular structures, and can be calculated when there is no clear picture of nominal stress due to complex geometry.
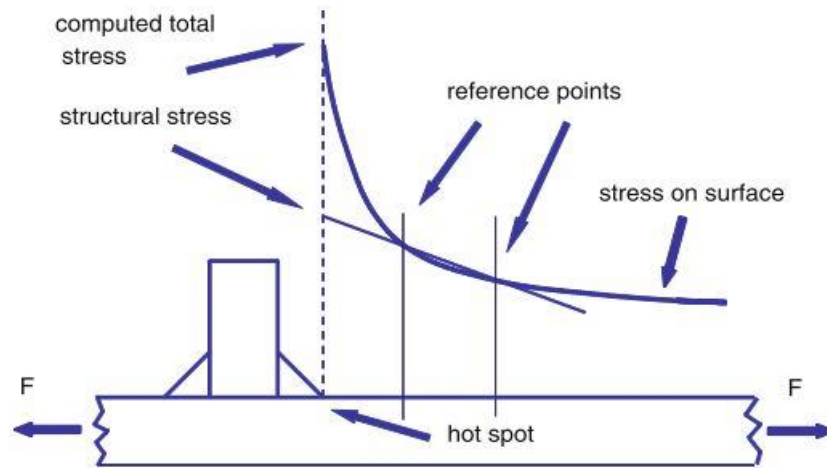
Fig. 29. Structural hot spot (SHS) definition

Most of the cases, this method is limited to the assessment of weld toe. On the other stress concentration factors are used, which is dependent on dimensional and geometric parameters. Principle stresses act perpendicular to the weld toe within $\pm\ 60^0$ for biaxial stress state of the plate surface.

5.2.3. Calculation of hot spot stress

There are two types of hot spot stresses as per the plate location and orientation with respect to weld toe, type a and type b see in **Fig.** 30. Welded component showing hot spots of types a and b. Structural stress can be calculated using finite element analysis by the extrapolation method. The non-linear peak should avoid by linearization of the stress through-thickness and extrapolation stress point at the surface to the weld toe. Two or three reference points might take for the determination of structural hot spot stress. Either thin plate or shell element or solid element may be applied to evaluate structural hot spot analysis. Stress closes to the nodal points are calculated as the first nodal point, and the refinement should also be done through-thickness direction. Shell mesh size should not exceed the width size of the weld joints, stress extrapolation for different meshes, and their evaluation methods are shown in **Fig. 31.** Stress Extrapolation with different meshing type a and type b, methods are shown in **Table 8**.

The structural hot spot S-N curves are stated in the same IIW design curves. The FAT number corresponds to the allowable stress range in MPa with the life of 2 x 10^6 fatigue life, however, the FAT numbers are different, and general form of equations for S-N curve (32) as shown below-

$$\Delta\sigma_{hs}^{m}.N = C \tag{32}$$

FAT is the fatigue class at a strength of 2x 10^6 cycles,

m is the slope of the upper part of the design curve

$\Delta\sigma_{hs}^{m}$ is the structural hot spot stress range

N is the number of cycles o failure

C is the design of fatigue capacity ($2x\ 10^6$ FAT^m)
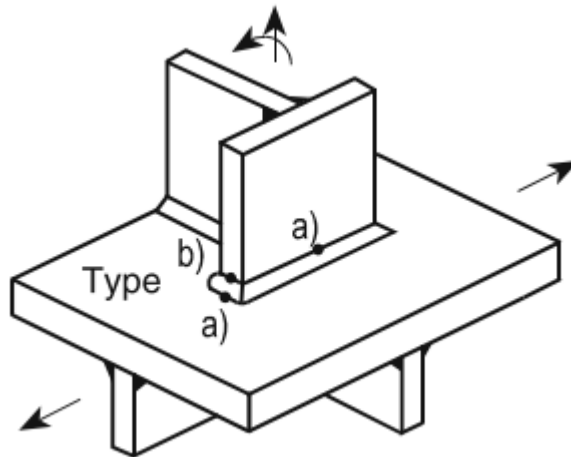
Fig. 30. Welded component showing hot spots of types a and b
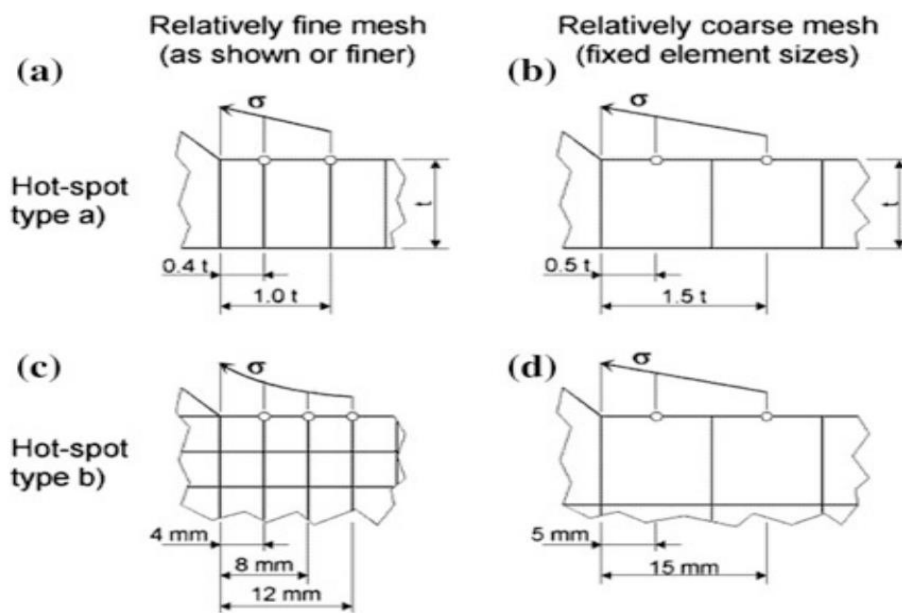
Fig. 31. Stress Extrapolation with different meshing type a and type b

Table 8. Extrapolating point evaluation methods for Type a and Type b

Model type		Coarse models		Fine models	
		Type-a	Type-b	Type-a	Type-b
Element size	Shells	t x t max t x w/2	10 x 10 mm	≤0.4t x t or ≤0.4t x w/2	≤4 x 4 mm

	Solids	t x t max t x w/2	10 x 10 mm	≤0.4t x t or ≤0.4t x w/2	≤4 x 4 mm
Estimated points	Shells	0.5 t and 1.5 t mid-side points	5 and 15mm mid side points	0.4 t and 1.0 t nodal points	4,8 and 12-mm nodal points
	solids	0.5 and 1.5 t surface centre	5- and 15-mm surface centre	0.4t and 1.0 t nodal points	4,8 and 12-mm nodal points

5.2.4. Stress extrapolation

– For type a (33), for fine mesh element, the evaluation of structural hot spot using the reference point. The evaluation of nodal stresses at two points 0.4 t and 1.0 t, the equation of structural hot spot stress as follows [20]. In **Fig. 32**. Shows the coarse and fine mesh elements of Submodel-3 with an element size of fine mesh not more than 4mm and coarse mesh 8mm.

$$\sigma_{h_s} = 1.67.\,\sigma_{0.4.t} - 0.67.\,\sigma_{1.0.t} \tag{33}$$

– For fine mesh evaluation of nodal stresses at three points 0.4 t, 0.9 t, and 1.4 t and 0.5 t, 1.5 t, and 2.5 t with a mesh size of the element, not more than 0.4 t, this method is used for the non-linear structural stress, sharp changes in the direction of applied force or structures with thick-walled

$$\sigma_{h_s} = 2.52.\,\sigma_{04t} - 2.24.\,\sigma_{09t} + 0.72.\,\sigma_{1.4t} \tag{34}$$

$$\sigma_{h_s} = 1.875.\,\sigma_{0.5t} - 1.25.\,\sigma_{1.5t} + 0.375.\,\sigma_{2.5t} \tag{35}$$

– The length of the coarse (36) mesh higher-order element is equal to the plate thickness *t*, the point evaluation at the surface centre or mid-side points, and for tubular joint wall thickness, the reference points are at 0.5 t and 1.5 t.

$$\sigma_{h_s} = 1.50.\,\sigma_{0.5t} - 0.50.\,\sigma_{1.5t} \tag{36}$$

– Structural stress Concentration factors
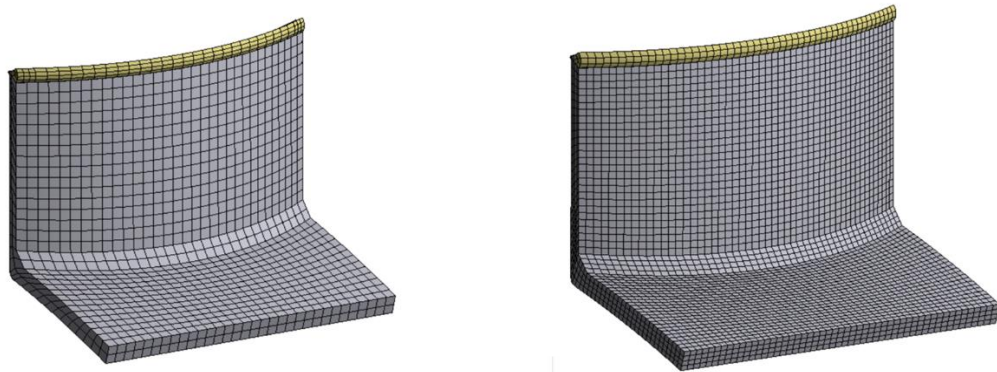
Fig. 32. Shows the coarse and fine mesh elements of Submodel-3

The structural stress concentration factor (k_s) (37) is the ratio of maximum structural stress (σ_s) to the nominal stress (σ_n). [21]

$$k_s = \sigma_s / \sigma_n. \tag{37}$$

In the case of hot spot structural stress (σ_{hs}), the equation would become

$$k_{hs} = \sigma_{hs} / \sigma_n. \tag{38}$$

The total hot spot stress(39) composed of axial and bending moments:

$$\sigma_{hs} = \sigma_{na}.K_{hs.a} + \sigma_{nb}.K_{hsb} \tag{39}$$

$K_{hs.a}$ − stress concentration factor related to axial stress

$K_{hs.b}$ − stress concentration factor related to bending stress

The structural stresses are maximum when the sudden changes of shape in the structure, such as at notches of the weld, and cracks may initiate at that points [22]. Fatigue strength assessment of ship structures explained in the article, which includes I section and double bottom section in a multi-box design [23] .

The hot spot stress concertation factors derived by Miki and Tateishi from section girders with cope holes [24], which might be applicable for flange cover plates, gusset plates, and some structural wildings. Weld notch stress increases with mesh size **Fig. 33** with k_{hs} stress concentration factor, and the hot spot stress concentration factor is calculated using two or three reference points see in **Table 9.** Calculated value of Structural hot pot stress for coarse and fine mesh. The structural stress is coming constantly from 2 mm-3 mm distance from the weld toe.

Table 9. Calculated value of Structural hot pot stress for coarse and fine mesh

Structural Detail	Mesh type	Structural Hot spot stress (σ_{h_s}) (MPa)	Hot spot stress concentration factor(k_{hs})
Submodel-3	Coarse	180.7	1.1510
	Fine	186.8	1.1601
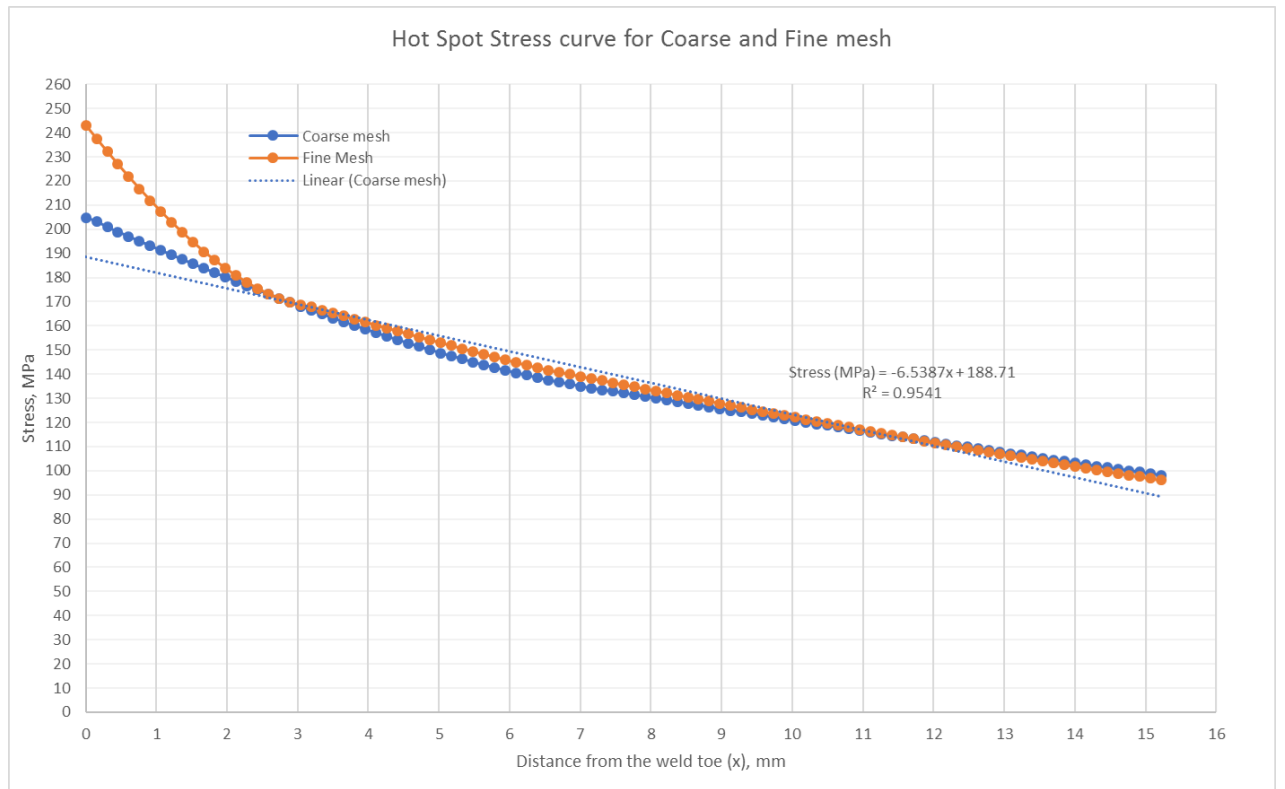
Fig. 33. Hot Spot Stress Curve for Coarse and fine Mesh of the model

For type b, the plate thickness does not depend on the stress distribution, so the extrapolation point weld is in absolute distance from the weld toe.

- For fine mesh the mesh element size would not be more than **4 mm** (40), in such a way that reference point can take at three normal distances 4mm, 8mm, 12 mm distances.

$$\sigma_{h_5} = 3.\sigma_{4\text{mm}} - 3.\sigma_{8mm} + \sigma_{12mm} \tag{40}$$

- The element length in the coarse mesh is **10 mm** (41), evaluation of the points from the mid-side of the element extracted using a linear extrapolation method.

$$\sigma_{h_5} = 1.5\sigma_{5mm} - 0.5.\sigma_{15mm} \tag{41}$$

5.2.5. Some alternative methods

There are several different methods to extract structural hot spot stresses which would be optional for exceptional cases, in Haibach 3 mm at a certain distance from the weld toe, further modified to stresses determined 2.0 mm-2.5 mm away from the weld toe, Atzori and Meneghett [25] clarified as 2.0-3.0 mm on the other hand by Xiao and Yamada, and stresses can be extracted 1.0 mm below the weld toe and using FEA methods.

Dong and Hong's special cases, partially from the hot spot and partially fracture mechanics, considered for evaluation of structural stresses, linearized stress distribution over plate thickness, and membrane and bending stresses to predict the crack formation within the depth of t1 (t1=t/2). Hot spot stress very much applicable for offshore and marine structures [22], roof stresses, and support

towers. A reliable way to define hot spot structural stresses to achieve a single define solution [26] assessed the welded joints of ship structures. The notch stresses are strictly depending on the continuum solid mechanics, which not be possible in hot spot structural stresses. Atzori suggested some 'v' notch at the weld toe, so the blunt equivalent notch combine with sharp 'v' notch. And it showed that it is not possible to separate structural stresses at the notch stresses with a sperate distance from the weld toe. It might be possible to derive the fatigue relevant notch stress intensity factor from the hotspot structural stress approach.

The structural stress corresponding to recommended endurable strain or structural stress is $\Delta_{\sigma_s} = 80$ N/mm^2 with a failure probability of $P_f = 0.01\%$ with an average cycle of 2×10^6, including weld high tensile strength [27], whereas endurable cycle strain is $\Delta\varepsilon_s = 0.06 - 0.14\%$ .Endurable structural stress or the equivalent stress Δs_s (N/mm^2) in the Dong and Xiamo approaches [28] as calculated and the structural stresses (42) are compared total peak stresses at the weld toe through-thickness 8 mm of the shell which as shown in **Fig. 34**.

$$\Delta s_s == \frac{\Delta\sigma_s}{[I(\delta_b)^{1/m}]}\left(\frac{t}{t_0}\right)^{1/2-1/m} \tag{42}$$

Almost 1mm depth, Total stresses and structural stresses are intersecting.
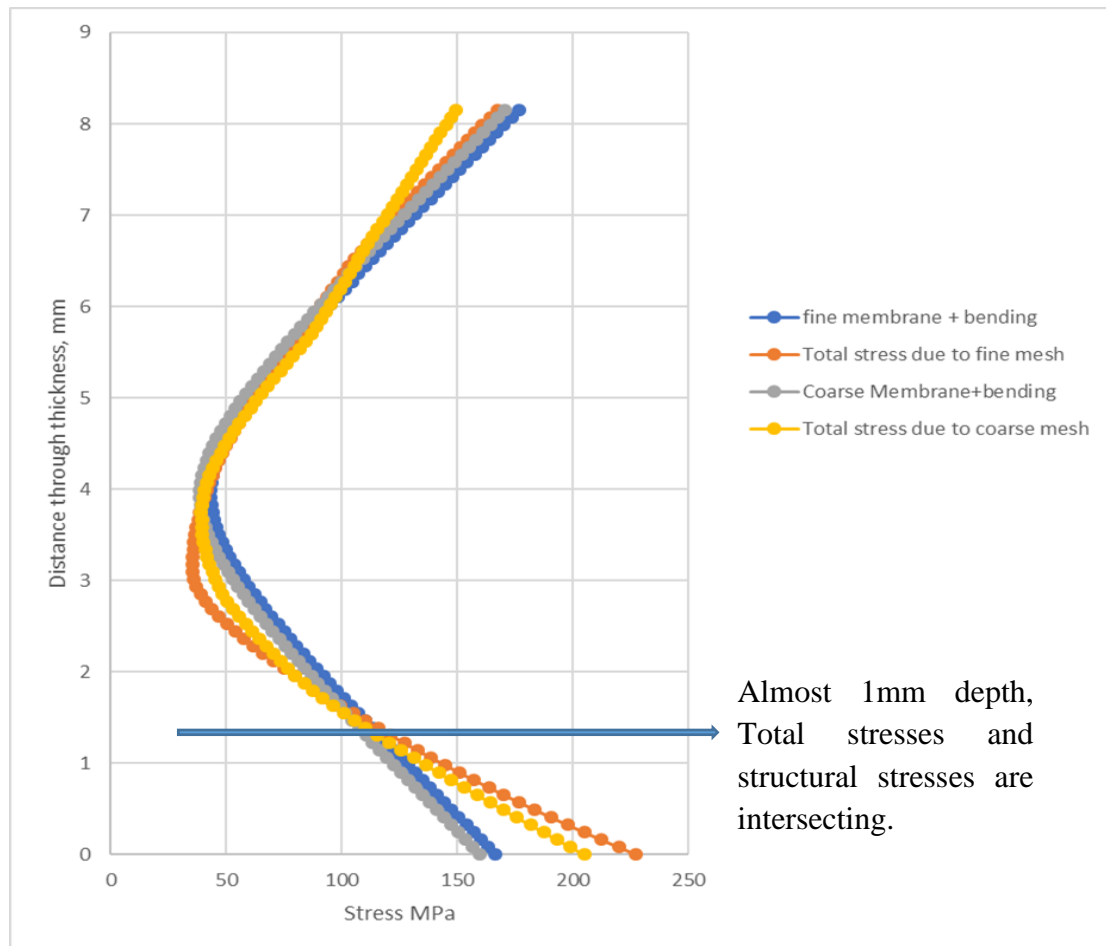
Fig. 34. Structural stress Vs Total stress through the thickness of the shell for coarse and fine mesh
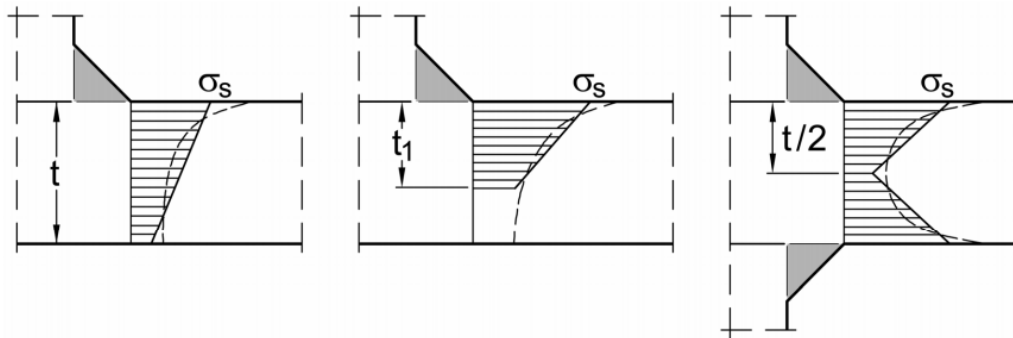
Fig. 35. Definition of structural stresses by Dong in different cases
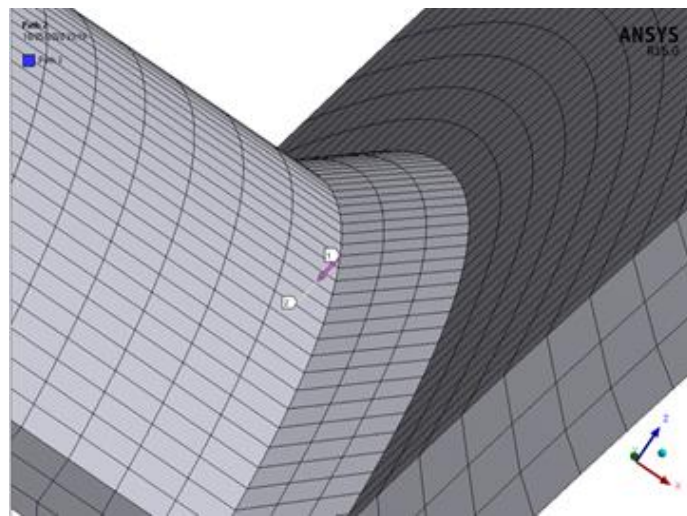
Fig. 36. Structural stress range extrapolation method though thickness of the shell from ANSYS

$\Delta\sigma_s$= 161 MPa from **Fig. 34**. is the way to find structural stress range from hot spot, stress analysis as shown in **Fig. 35**. and **Fig. 36**., which is an endurable structural stress or strain, m=3.6 by Dong, Plate and wall thickness t, with reference thickness t_0 the crack growth integral I, δ_b is the ratio of bending to total stress ratio. This method is purely insensitive to meshing in finite element analysis. [29][30].

5.2.6. Effective notch Stress Method

The effective notch stress is the total stress produced at the root of the notch, which is assumed as a linear elastic material. The weld shape parameters, including the notch radius and root of the weld, are replaced with an effective notch radius r=1 mm. [27] see in **Fig. 37**. This method is limited to the weld toe, and roots have effective notch stress of at least 1.6 times that of structural hot spot stress. It covers the structural hot spot stress, but the other modes, such as fatigue failure due to crack growth in the surface, are excluded. The effective notch radius stress is compared with the universal S-N diagram, FAT class 225.see in **Fig. 39**. The effective notch and root radius of 1mm applicable for material which has greater than 5mm thickness. The weld should have a flank angle of 450 for fillet welds and 300 for butt welds. Machined or ground weld profile is possible to assess the notch stress of the actual profile. If the material is less than 1mm thickness 0.05 and 0.03mm, effective notch radiuses are applicable.[31]
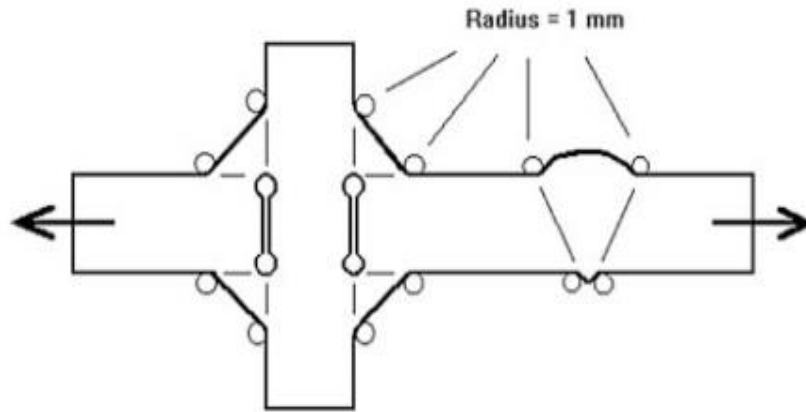
Fig. 37. Fictious notch rounding radius with 1mm

    – Calculation of effective notch stress

The effective notch stress can be calculated with the help of finite element analysis, the recommended element sizes at the notch radius as follows in the **Fig. 38**

Element type	Relative size	Absolute size [mm]	No. of elements in 45° arc	No. of elements in 360° arc
Quadratic with mid-side nodes	$\leq r/4$	≤ 0.25	≥ 3	≥ 24
Linear	$\leq r/6$	≤ 0.15	≥ 5	≥ 40

Fig. 38. Recommended Element sizes at the effective notch radius

For effective notch stress analysis, for linear elements, the element sizes should not be more than that of 1/6 of the radius and ¼ of radius for higher-order elements. The elements should be calculated at the curved portion of the radius, which is either tangential or normal to the surface. It is possible to convert t 3D to 2D with two conditions: the loading is perpendicular to the weld joint, and the normal and shear stress is considered to be neglected. Secondly, the loading and geometry of the assessment weld area should not be changed. The maximum principle stresses are used in case of multiaxial stresses, which should provide negative or positive minimum principal stresses. The photo-elastic stress measurements are used to measure the effective notch.

The fatigue strength of a material heavily depends upon the notch effect, which means the stress concentration and strength reduction by notches. The notch effect depends on the shape of the weld geometry. In the case of sharp notches at the weld toe, microstructural notch stress considers, which means grain structure, microfilming, and crack initiation of the small volume or area can determine the stress concentration effect.

The stress averaging approach used in the form of fictious notch rounding, which is applicable for notch tips with distinct area or volume. The notch stress methods are appropriate for fracture mechanics, crack propagation and to analyse fatigue strength of the whole component. Short crack

behaviour at the sharp notches, Topper and El Haddad. [32], a* which supports the stress intensity factor Δk_{th}.

In the case of multiaxial stresses, the von mises distortion energy criteria are considered with non-varying principle stresses, which assumes the material's ductility. More complicated criteria are assumed in cases of multi-axial notch stresses [33].

The most recent development of the stress approach is the effective notch radius approach with ρ =0.05-0.1mm, which is applicable for thin sheet structures, whereas traditional notch stress is derived from an unnotched specimen limited to specified thickness. The notch stress approaches also applicable to the non-welded components. A normal notch stress approach is used when the nominal stress approach and hot-spot stress is not applicable joints. To get a finite life of the structure the notch stress approach should combine with the crack propagation approach and notch strain approach.

The distance approach is developed to evaluate the fatigue life of welded components, which is applicable for both seam and spot-welded joints. This has a notch factor with the initial crack depth ai=0.25mm, elastic-plastic notch stress analysis considers, and up to final fracture.

The [34] elastic stress concentration factor, to analysis the crack initiation life, which is performed with a cross-sectional area of the weld joint with simple engineering formulas.

$$K_f = 1 + \frac{K_t - 1}{1 + \dfrac{a^*}{\rho}}$$
(43)

The fatigue notch factor K_f (43) which is derived from fatigue stress concentration factor K_t, where the factor is lower when sharp notches occurred. The value depends upon the ratio $\dfrac{a^*}{\rho}$, where a^* is the material constant and ρ is the notch radius of the weld joint. The maximum fatigue notch factor K_f occurs when $a^* = \rho_c$, where ρ_c is the critical notch factor. In the case of worst-case condition for deep elliptical notch, the stress concentration factor K_f is depends upon $\sqrt{\dfrac{1}{\rho}}$, and the material constant $4a^* = \rho$ from Neuber's worst-case analysis theory which means that the notch radius is 1mm and $a^* = 0.25$.

The Fictious notch radius approach is applicable for both seam and spot-welded joints, especially for low strength steels. The sharp notches introduce in order to obtain maximum notch stress with reference to the nominal stress. The fictious notch radius ρ_f (44) with real notch radius ρ , multiaxiality coefficient **s** and material constant ρ^* which together forms equation

$$\rho_f = \rho + s\rho^*$$
(44)

the maximum fatigue effective notch stress should compare with the endurance limit of the parent material. In the case worst case condition, the real notch radius is considered as zero, so the fictious notch radius would become one $\rho_f = 1$. [24]

The crack initiation with high cycle range when calculating the fatigue notch factor by Lawrence with N>10^5 which is related to the traditional method of N>10^7 which is reviewed by notch strain approach.

The fatigue strength reduction factor commonly used for welded joints, the correction factor must be introduced when calculation fatigue notch factor, or low alloy steel it is 1/0.9.

Based on Neuman for low strength structural steel $\Delta\sigma_E$ endurable stress range is 240N/mm2 with $N = 2 \times 10^6$, cycles so that $\Delta\sigma_{nE} = \frac{240}{0.9K_f}$,.

Modified notch rounding approach: -

The reliability of the type of structural steel $\sigma_{y_{0.2}} = 375 - 485 \ N/mm2$

Highly stress volume approach influences the size effect of the notch root affects the multiaxial local stresses with crack initiation of considered ai=0.5-1 mm, which depends upon the local volume of highly stressed material. The maximum notch root stress up to 90% from normalised stress, only with the effect of change in notch radius. And different angle is considered at the notch radius to describe the crack initiation.

The microstructural changes at the weld to depends upon the fatigue notch factor. The notch stress amplitude which is the product of notch factor and nominal stress amplitude.
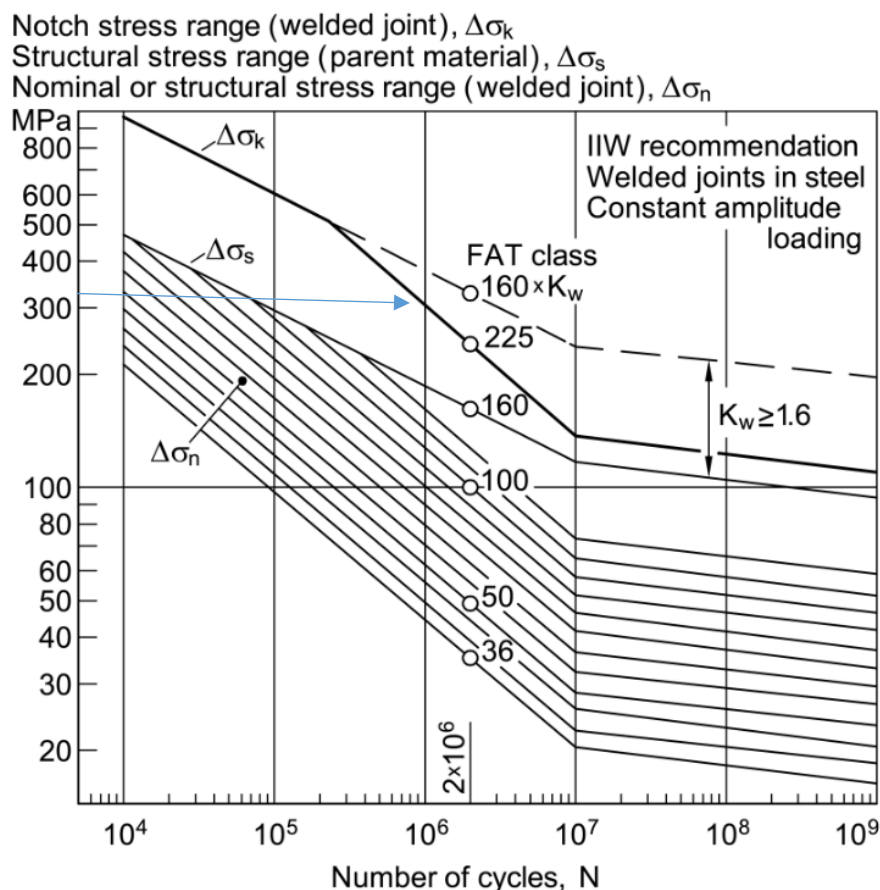
Fig. 39. SN Curves of fatigue classes in terms of FAT 225

The effective notch stress with a radius of 1mm recommended by IIW standards with different size of notch elements is calculated. This is the most accurate way of calculating structural stress which can see in **Fig. 40.** The Graph shows the maximum stresses with different element numbers at 1mm

notch radius. With increasing the mesh element, the notch stresses get distributed along the weld toe notch as shown in **Fig. 41.** Number of elements is showing at notch radius, and refining the notch element would not affect the structural stress range of the component.
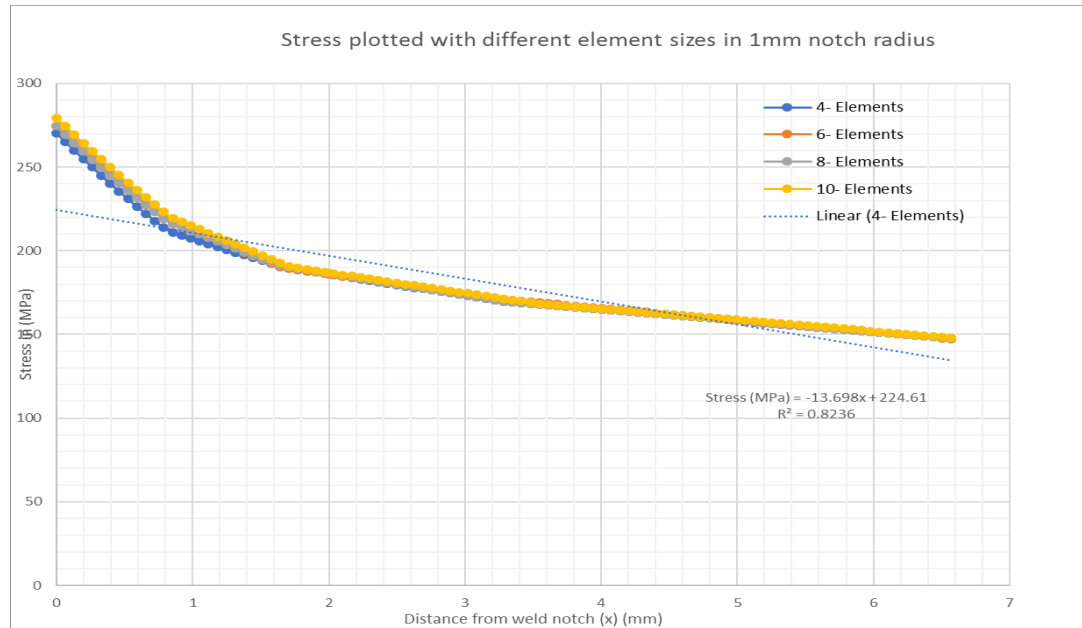
Fig. 40. The Graph shows the maximum stresses with different element numbers at 1mm notch radius
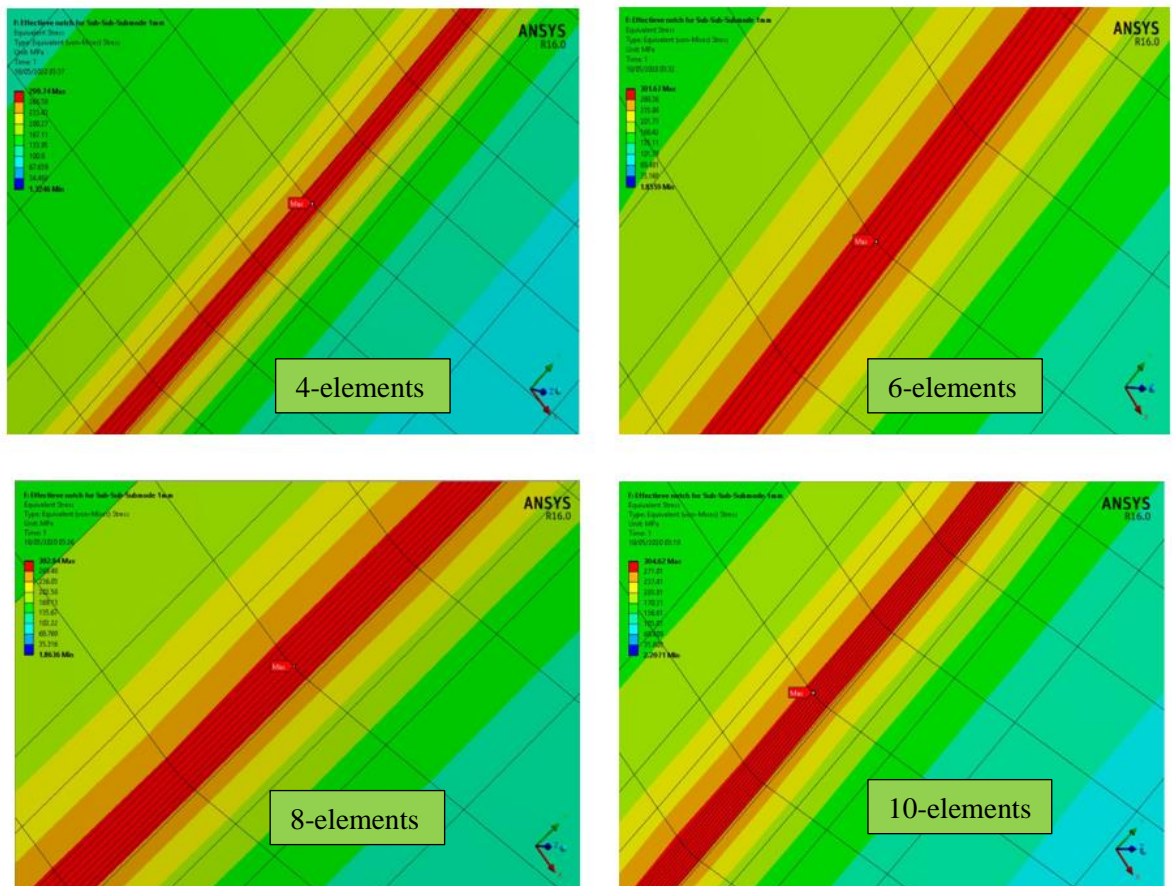
Fig. 41. Number of elements is showing at notch radius

Conclusions

1. Reviewed the design codes and standards for the construction of surge tank and analyse various parts, and classes of weld joints in the vessel. Calculated the optimal thickness of the shell as 8 mm, and for head considered as 2:1 ellipsoidal with a nominal thickness of 10 mm. This allows working of surge tank with a range of 0 to 0.345 MPa. The reinforcement pad with a suitable area of element would be 636 mm2, and the weld load is maximum in the direction of W33, which is three times greater than the lowest one.

2. Studied the stress distribution of surge tank and FEA modelling. Examined the mesh modelling approach of shell and solid elements at the weld toe region of the vessel. The maximum stress is identified at the manhole nozzle which is about 165.68MPa. The manhole nozzle is the largest nozzle and opening of the vessel where the chances of fatigue failure in this region is highest compared to other parts of the vessel.

3. The study of sub-modelling technique in finite element modelling software shows the interpolation of nodal displacements from the global model to the sub-models are accurate. This is one of the most controlling methods in finite element analysis for detailed analysis of the area of interest, and the selection of the area of interest entirely depends upon the user. Studied the most advanced finite element software that supports the sub-modelling technique. Examined the results and verified the reliability of this technique.

4. The Fatigue assessment procedure is carried out based on recent articles and international standards. From ASME, Effective equivalent stress amplitude determines the fatigue life using the elastic approach. On the other hand, for weld assessment, the structural stress determined fatigue life, which is insensitive to the mesh sizing in FEA. Considered three local approaches and some external methods from IIW standard for the fatigue assessment of weld joints. The nominal stress approach is a conventional method, and for hot spot analysis, structural stresses are extrapolated with respect to the referral points Infront of the weld toe region. The nominal and hot spot stress analysis would change with the structural stresses of the domain with a variation of mesh size due to an increase in stress concentration at the weld toe region. Dong and Xiamo approaches are insensitive to meshing in finite element analysis, and the structural stresses might not vary with element size (should not less than four elements) at the notch from effective notch stress analysis. The design codes are limited to some thickness, types of joints and materials of the component. The number of cycles calculated from ASME is 1.2×10^5. On the other hand, from a hot spot and nominal stress analysis showed almost 2.5×10^5. The effective notch stress analysis indicated a survival probability of 86.2% compare with two million cycles of steel survival probability of 90%.

List of references

1. RINGSBERG, Jonas W., ANVARI, Majid, DJAVIT, Djan Eirik and STRANDE, Erik. Fatigue failure analysis of fillet welded joints used in offshore structures. *Proceedings of the International Conference on Offshore Mechanics and Arctic Engineering - OMAE*. 2014. Vol. 4A. DOI 10.1115/OMAE2014-23166.
2. ASME. ASME Boilers and Pressure Vessel Code. . 2019. P. 651–652.
3. MODULE, I A B. Design of welded pressure equipment. . 2017. No. 1998, p. 1–65.
4. NIRANJANA, S. J., PATEL, Smit Vishal and DUBEY, Ankur Kumar. Design and Analysis of Vertical Pressure Vessel using ASME Code and FEA Technique. *IOP Conference Series: Materials Science and Engineering*. 2018. Vol. 376, no. 1. DOI 10.1088/1757-899X/376/1/012135.
5. DAY, B. V. Fatigue Analysis of Pressure Vessels. *Transactions of the International Conference on Structural Mechanics in Reactor Technology*. 1981. Vol. 13, no. 1, p. 25–28.
6. ASME.II, Section.ASME Section ii 2017. . 2017.
7. CHATTOPADHYAY, A., GLINKA, G., EL-ZEIN, M., QIAN, J. and FORMAS, R. Stress analysis and fatigue of welded structures. *Welding in the World*. 2011. Vol. 55, no. 7–8, p. 2–21. DOI 10.1007/BF03321303.
8. ASME. ASME VIII Division 2 - Alternative Rules - RULES FOR CONSTRUCTION OF PRESSURE VESSELS. . 2017. P. 867. DOI 10.1016/b978-0-323-34126-4.00063-3.
9. NARVYDAS, E and PUODZIUNIENE, N. Applications of Sub-modeling in Structural Mechanics Applications of Sub-modeling in Structural Mechanics. . 2015. No. April 2014.
10. NOTES, Abaqus Release, INSTALLATION, Abaqus, GUIDE, Licensing and NOTES, Abaqus Release. Abaqus Volume Ii: Analysis. . 2016. Vol. II.
11. CUNNINGHAM, Patrick. Submodeling using ANSYS Workbench. *Workbench*. 2011.
12. SPT GROUP. Dynamic Multiphase Flow Simulator. [online]. 2015. Available from: http://www.sptgroup.com/upload/documents/Brochures/Transient-Well-Flow-Simulations.pdf
13. GONZÁLEZ-ALBUIXECH, V. F., QIAN, G., SHARABI, M., NIFFENEGGER, M., NICENO, B. and LAFFERTY, N. Comparison of PTS analyses of RPVs based on 3D-CFD and RELAP5. *Nuclear Engineering and Design* [online]. 2015. Vol. 291, p. 168–178. DOI 10.1016/j.nucengdes.2015.05.025. Available from: http://dx.doi.org/10.1016/j.nucengdes.2015.05.025
14. GIGLIO, M. FEM submodelling fatigue analysis of a complex helicopter component. *International Journal of Fatigue*. 1999. Vol. 21, no. 5, p. 445–455. DOI 10.1016/S0142-1123(99)00002-X.
15. ARISTOVICH, K. Y. and KHAN, S. H. A new submodelling technique for multi-scale finite element computation of electromagnetic fields: Application in bioelectromagnetism. *Journal of Physics: Conference Series*. 2010. Vol. 238, no. July 2010. DOI 10.1088/1742-6596/238/1/012050.
16. MADGE, J. J., LEEN, S. B. and SHIPWAY, P. H. A combined wear and crack nucleation-propagation methodology for fretting fatigue prediction. *International Journal of Fatigue*. 2008. Vol. 30, no. 9, p. 1509–1528. DOI 10.1016/j.ijfatigue.2008.01.002.
17. ALBUQUERQUE, Carlos, SILVA, António L.L., DE JESUS, Abílio M.P. and CALÇADA, Rui. An efficient methodology for fatigue damage assessment of bridge details using modal superposition of stress intensity factors. *International Journal of Fatigue* [online]. 2015. Vol. 81, p. 61–77. DOI 10.1016/j.ijfatigue.2015.07.002. Available from: http://dx.doi.org/10.1016/j.ijfatigue.2015.07.002
18. HEYES, Peter and MENTLEY, Jeff. Fatigue Analysis of Seam Welded Structures using nCode DesignLife. *nCode*. 2013. P. 1–21.
19. PATIL, Rakesh and ANAND, Soham. Thermo-structural fatigue analysis of shell and tube type heat exchanger. *International Journal of Pressure Vessels and Piping* [online]. 2017.

Vol. 155, p. 35–42. DOI 10.1016/j.ijpvp.2017.03.004. Available from: http://dx.doi.org/10.1016/j.ijpvp.2017.03.004

20. HOBBACHER, A. F. *Erratum to: Recommendations for Fatigue Design of Welded Joints and Components*. 2019. ISBN 9781855733152.

21. DELEGATION, British and NIEMI, By E. XIII-2639r3-16 STRUCTURAL HOT-SPOT STRESS APPROACH TO. . 2016.

22. GARBATOV, Y., RUDAN, S., GASPAR, B. and GUEDES SOARES, C. Fatigue assessment of marine structures. *Marine Technology and Engineering*. 2011. Vol. 2, no. September 2014, p. 865–888. DOI 10.13140/RG.2.1.3185.0488.

23. HAMMERSTAD, Benedicte Hexeberg, SCHAFHIRT, Sebastian and MUSKULUS, Michael. On Fatigue Damage Assessment for Offshore Support Structures with Tubular Joints. *Energy Procedia* [online]. 2016. Vol. 94, no. January, p. 339–346. DOI 10.1016/j.egypro.2016.09.193. Available from: http://dx.doi.org/10.1016/j.egypro.2016.09.193

24. MASCHINENBAU, Vom Fachbereich and MORGENSTERN, Dipl Christoph. Kerbgrundkonzepte für die schwingfeste Auslegung von Aluminiumschweißverbindungen am Beispiel der. *Design*. Vol. 6.

25. ATZORI, B., BLASI, G. and PAPPALETTERE, C. Evaluation of fatigue strenght of welded structures by local strain measurements. *Experimental Mechanics*. 1985. Vol. 25, no. 2, p. 129–139. DOI 10.1007/BF02328802.

26. FRICKE, Wolfgang and KAHL, Adrian. Comparison of different structural stress approaches for fatigue assessment of welded ship structures. *Marine Structures*. 2005. Vol. 18, no. 7–8, p. 473–488. DOI 10.1016/j.marstruc.2006.02.001.

27. A. HOBBACHER. IIW document IIW-1823-07 FATIGUE DESIGN OF WELDED. . 2008.

28. DONG, P. A structural stress definition and numerical implementation for fatigue analysis of welded joints. *International Journal of Fatigue*. 2001. Vol. 23, no. 10, p. 865–876. DOI 10.1016/S0142-1123(01)00055-X.

29. KIM, Myung Hyun, KIM, Seong Min, KIM, Young Nam, KIM, Sung Geun, LEE, Kyoung Eon and KIM, Gyeong Rae. A comparative study for the fatigue assessment of a ship structure by use of hot spot stress and structural stress approaches. *Ocean Engineering* [online]. 2009. Vol. 36, no. 14, p. 1067–1072. DOI 10.1016/j.oceaneng.2009.07.001. Available from: http://dx.doi.org/10.1016/j.oceaneng.2009.07.001

30. SEYEDI, Alireza and GULER, Mehmet Ali. Mesh Insensitive Structural Stress Method for Fatigue Analysis of Welded Joints Using the Finite Element Method Mesh Insensitive Structural Stress Method for Fatigue Analysis of Welded Joints Using the Finite Element Method. *th International Advanced Technologies Symposium (IATS'17)*. 2017. No. October.

31. FRICKE, Wolfgang. IIW Recommendations for the Fatigue Assessment of Welded Structures By Notch Stress Analysis: IIW-2006-09. *IIW Recommendations for the Fatigue Assessment of Welded Structures By Notch Stress Analysis: IIW-2006-09*. 2012. P. 1–41. DOI 10.1533/9780857098566.

32. EL HADDAD, M. H., SMITH, K. N. and TOPPER, T. H. Fatigue crack propagation of short cracks. *Journal of Engineering Materials and Technology, Transactions of the ASME*. 1979. Vol. 101, no. 1, p. 42–46. DOI 10.1115/1.3443647.

33. SONSINO, C. M. and KUEPPERS, M. Multiaxial fatigue of welded joints under constant and variable amplitude loadings. *Fatigue and Fracture of Engineering Materials and Structures*. 2001. Vol. 24, no. 5, p. 309–327. DOI 10.1046/j.1460-2695.2001.00393.x.

34. FATIGUE, Predicting T H E and WELDS, Resistance O F. PREDICTING THE FATIGUE Stress Analysis of Weldments. . 1981. P. 401–426.

Appendix 1: An AutoCAD drawing of the Surge tank welded model

Appendix 2: MATLAB calculated values

```
Editor - D:\D\KTU\KTU\SEMESTER 4\RESEARCH FINAL\Matlab\New folder\ASME WELD\ASME_DIVION2_FATIGUE_LIFE_CYCLE_Final.m

effectieve_notch_stressnn.m   ASME_DIVION2_WELD_fatigue_assessmentn.m   ASME_DIVION2_FATIGUE_LIFE_CYCLE_Final.m   nominal_Stress.m   hot_spot_stress_new.m   +

18     C4=6.654000E-02;%ksi
19  -  c5=2.020834E-1;%ksi
20  -  c6=-6.940535E-03;%ksi
21  -  c7=-2.079726E-02;%ksi
22  -  c8=2.010235E-04; %ksi
23  -  c9=7.137717E-04; %ksi
24  -  c10=0;
25  -  c11=0;
26  -  cus=1;
27  -  Efc=28282.3589;%ksi195000;%Mpa
28  -  Et=28951.9981;%ksi199617;%Mpa
29     % sa=30.7%MPa
30     % Y=log(28300*(207.1080/0.0073))
31     % Y1=log(28.3E3*(sa/Et))
32  -  Y=(Saltk/cus)*(Efc/Et);
33  -  X=(c1+c3*Y+c5*Y^2+c7*Y^3+c9*Y^4+c11*Y^5)/(1+c2*Y+c4*Y^2+c6*Y^3+c8*Y^4+c10*Y^5)  %10^Y>=20
34  -  N=10^X
35
36  -  Fatige_damage_factor=10000/N
37
38     %samplecalcultion of primary membrane stress
39     % P=0.4;
```

```
Command Window

N =

   1.2022e+05


Fatige_damage_factor =

   0.0832
```

```
Editor - D:\D\KTU\KTU\SEMESTER 4\RESEARCH FINAL\Matlab\New folder\ASME WELD\ASME_DIVION2_WELD_fatigue_assessmentn.m

effectieve_notch_stressnn.m   ASME_DIVION2_WELD_fatigue_assessmentn.m   ASME_DIVION2_FATIGUE_LIFE_CYCLE_Final.m   nominal_Stress.m   hot_spot_stress_new.m   +

1  -  clc;
2  -  clear all;
3  -  eps_k=0.00072543% neubers rule
4  -  Sigm_k=200000/(1-0.28^2)*eps_k
5  -  Sigm_k=162%27.55%ksi
6  -  m_ss=3.6;
7     % E=I^(1/m_ss);
8  -  x=(2-m_ss)./(2*m_ss)
9  -  Rbk=150/(150+42);
10 -  t_ess=16;%0.625;
11 -  fMK=1;
12 -  E=(1.23-0.364.*Rbk-0.17.*Rbk.^2)./(1.007-0.306.*Rbk-0.178.*Rbk.^2)
13 -  I=(E)^(1/m_ss);
14     %ds=(Sigm_k)/(t_ess)^x*(I)*fMK
15 -  ds=(Sigm_k)/(t_ess)^x*(I)*fMK
16     %ds=350
17 -  fe=1 ;%environmental correction factor
18 -  f_mt=1  ;%material and tempature correction factor Et/Eacs
19 -  C=11577;%19930.2 ; %equation constant used to represet smooth fatigue curves
20     %sa= 80 ;%Mpa Computed equivalent structural stress range parameter part 5
21 -  h=0.32;
```

```
Command Window

N =

   1.2961e+05


Fatige_damage_factor =

   0.0077
```

effectieve_notch_stressnn.m × ASME_DIVION2_WELD_fatigue_assessmentn.m × ASME_DIVION2_FATIGUE_LIFE_CYCLE_Final.m × nominal_Stress.m × hot_spot_stress_new.m × +

```matlab
28 -    Sigma_t1=157.8;%0.5t,4
29 -    Sigma_t2=112;%1.5t,12
30 -    Sigma_t3=167.165;%0.4t,3.2
31 -    Sigma_t4=133.67;%1.0t,8
32 -    Sigma_t5=148.36;%5mm
33 -    Sigma_t6=99.40;%15mm
34 -    Sigma_hs1= (1.5*Sigma_t1)-(0.5*Sigma_t2)%Mpa 179.6350OKKK COARSE MESH
35 -    Sigma_hs11=(1.67*Sigma_t3)-(0.67*Sigma_t4)%Mpa 190.8730OKKK FINE MESH
36      %Sigma_hs12=1.5*Sigma_t5-0.5*Sigma_t6% type b
37
38      %Quadratic extrapolation
39 -    Sigma_t21=150;%0.5t,4
40 -    Sigma_t22=100;%1.5t,12
41 -    Sigma_t23=80;%2.5t,20
42 -    Sigma_t24=170;%0.4t,3.2
43 -    Sigma_t25=140;%0.9t,7.2
44 -    Sigma_t26=100;%1.4t,11.2
45
46 -    Sigma_hs21= (1.875*Sigma_t21)-(1.25*Sigma_t22)+(0.375*Sigma_t23)%Mpa  186.2500
47 -    Sigma_hs22= (2.52*Sigma_t24)-(2.24*Sigma_t25)+(0.72*Sigma_t26)%Mpa 186.8000%%OKKK FINE MESH
48 -    t=8;%0.5t
```

Command Window

```
Sigma_hs1 =

  180.7000


Sigma_hs11 =

  189.6067
```

Appendix 3: Submitted for publication in conference "Industrial Engineering 2020" , Topic- "Application of Sub-modelling Technique in Surge Tank Welded Structure"

The International Young Researchers Conference
"INDUSTRIAL ENGINEERING 2020"

Application of Sub-modelling Technique in Surge Tank Welded Structure

Abdul khan THORAPPA[*]**, Evaldas NARVYDAS**[**]
* Kaunas University of Technology Studentu st. 56, LT-51424 Kaunas, Lithuania, E-mail: abdul.thorappa@ktu.edu
** Kaunas University of Technology, Studentu st. 56, LT-51424 Kaunas, Lithuania, E-mail: evaldas.narvydas@ktu.lt

1. Introduction

Sub-modeling is a model reduction technique in finite element analysis software that can concentrate on the local area and reduce the size of the complexity of the model during the calculation. The cut boundary conditions of the sub-model often are determined by the interpolation of the calculated nodal displacements of the global model. The cut boundary is the smaller model or an area of interest that is cut from the global modal, and the cut boundary purely depends upon the user. The calculation of the global model might require more time for calculation, and the result could be inaccurate. Therefore, the sub-model is cut from the global model to represent the domain for detail analysis (for construction purposes, fatigue assessments, weld analysis, fillets). Sub-models can be cut further into smaller sub-models to increase the accuracy of the calculation.

Sub-modelling approach is based on St. Venant's principle, which states that if an actual distribution of forces is replaced by a statically equivalent system, the distribution of stress and strain is altered only near the regions of load application. This principle states that when actual boundary conditions of the sub-model are replaced by the equivalent boundary conditions, there is no difference in the model response in the region, which is not close to the boundary of the sub-model. Although the sub-model size is determined by the user, the deformation should be checked with the global model so that the user can verify the model analysis.

There are two types of basic sub-modelling techniques to define the boundary condition of sub-model: 1) displacement-based sub-modelling and 2) force-based sub-modelling. In displacement-based sub-modelling, the displacements of the global model are transferred to the faces of the sub-model, where

it interacts with the global model. However, the major drawback of displacement-based sub-modelling is that the cut boundary displacements are valid only when the improvement of the sub-model does not change the stiffness comparing the initial global model. On the other hand, force-based sub-modelling reaction forces of the cut boundaries are transferred to the sub-model, which can be imported from the user-defined sources. The displacement-based sub-modelling are less sensitive to the mesh density of the global model [1].

Sub-modelling technique supports finite element software such as ANSYS, ABAQUS, Nastran, and integrated CAD/CAE software (SOLIDWORKS Simulation). The ABAQUS software allows nodal based and surface-based sub-modelling. In nodal based sub-modelling, the global nodal results are interpolated onto the sub-model to obtain surface traction, supporting a variety of element type combinations and procedures. On the other hand, in Surface-based sub-modelling only available for solid to solid in sub modelling in static. Convergence difficulties may occur in surface-based sub modelling, so inertia relief may be the solution [2]. Secondly, in ANSYS software, which is more advanced, less complicated, and allowing both nodal based and force-based sub-modelling for beam-to-solid, shell to solid (2D analysis to 3D analysis) and solid to solid (3D analysis to 3D analysis) sub-modelling system [3]. The sub-modelling technique could be successfully used not only for stress analysis but also for thermal, electromagnetic, and CFD analysis. Sub-modelling folder automatically created in ANSYS, which allows the definition of applied load, which would be either in displacement or body temperature, and this load must be applied to the cut boundaries of the sub-model, however, local body constraints should be defined in other parts of the sub-model. Finally, in SOLIDWORKS, the sub-modelling technique is a fully automated, less complicated, and global model treated as a separate component or part, and it might have an incompatible mesh with other regions [4]. Sub-modelling techniques can be useful in different engineering fields such as structural mechanics [5, 6], electromagnetics [7], fracture mechanics [8], fatigue assessment [5].

2. Materials and methods

2.1 Global model

The global model is a surge tank which is shown in Fig. 1 with a total height of 3.1 m and 2.3 m internal diameter. Shell and head material are carbon steel plates SA 516 Gr (485) 70, SA - meaning ASME Boiler and Pressure Vessel material specification versus A, which is for ASTM material specification; 516 – number selected for carbon steel pressure vessel plate material. Gr70 is the minimum strength grade of the carbon steel plate in ksi units. This material is most widely accepted for boilers, heat exchangers, pressure vessels, and storage tanks. It has a yield strength of 260 MPa and tensile strength of 485-650

MPa. Weld neck reinforcement flanges are SA 105M material, which is welded with carbon steel pipes (SA 106 Gr B). Weld geometry is designed according to international design codes and standards (ASME, EN 13445, IIW recommendations) and beveling according to AWS D1.1. The welding procedure follows
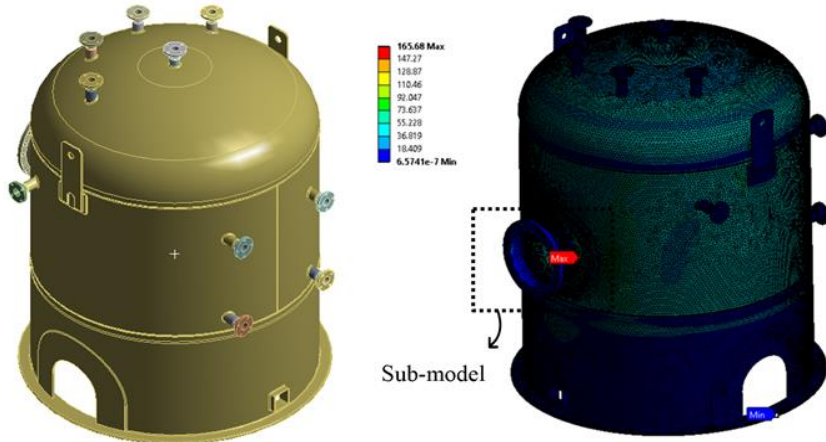

Fig. 1 Surge tank and its equivalent von Mises stress distribution which is maximum at manhole weld joint.

ASME Section IX standard. Nozzle weld root passes with GTAW (filler material ER 70S-2), cap pass with SMAW welding (filler material E7018). Usually, the filler materials used for welding have more tensile and yield strength compared to the base model [9].

The surge tank is operating with an inside pressure of 0.345 MPa, assuming negligible wind loads, and the vessel is fixed at the base ring. It allows deformation maximum at the manhole junction of the vessel, which is the largest opening and the largest nozzle of the vessel.

The surge tank has the capacity of 9320 litres, manufactured according to ASME Section VIII Division 1, and more detailed analysis follows according to ASME section VIII division 2 standards. Plate thickness of shell and dish end was calculated as 8 mm; however, for an ellipsoidal head of the vessel have 10 mm thickness for safety reason since stress concentration would be more at its curved configurations.

2.2 Sub-models

Fig. 2 shows the sub-models of the manhole nozzle part, which are extracted from the global model of the surge tank and transfer displacement from the global model to the sub-model. Sub-modelling plot increases the accuracy

of meshing and stress and strain distributions, which gives a clear idea of maximum allowable stresses at a critical point. The weld model was indicated in the sub-model, and it was clear that higher stress at the weld toe region and chances of failure more at that point. With the sub-modelling technique, the user can expect accurate mesh and a great option to study more about the critical joints such as welds, small fillets, chamfers, defects, and cracks.
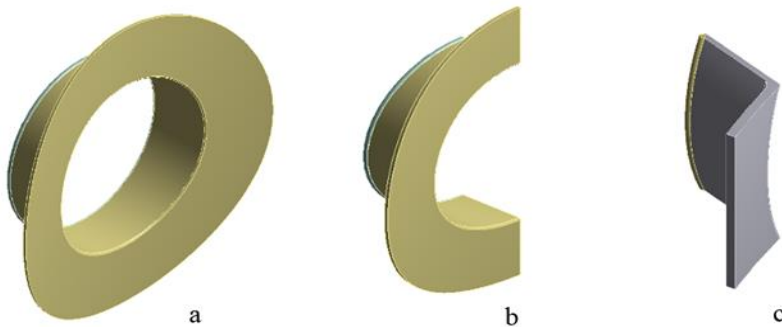

Fig. 2 Sub-models: a – sub-model 1 (an area of interest which is cut from global model), b – sub-model-2 (sub-model of sub-model-1) c – sub-model-3 (sub-model of the sub-model-2)

2.3 Sub-modeling procedure

1) The global model should be created and defined. Analysis should be done with appropriate meshing, and the area of interest should be defined.

2) The size of the sub-model should be defined by the user based on the area of interest, which should be sliced from the global model for sub-modelling analysis.

3) Sub-model is created by duplicating the global model and suppress all parts except the region of interest for detail analysis. The nodal displacement at the cut boundary must be derived from the global model.

4) Mesh refinement and model correction can be done with the sub-model for increasing the accuracy of the solution.

5) Nodal displacement from the global model should be inserted to the cut boundaries of the sub-model as the constraints and displacement should be inserted at this location, and the local boundary condition should define in the sub-model.

6) Sub-model analysis should perform and can expect higher level accuracy in the solution or repeat sub-modelling technique in the local model at an infinite number of times until to get accurate results.

3. Results and Discussions

Finite element analysis of a complex model mostly time-consuming, which might not get an accurate result. Sub-modelling techniques are precise for a complete analysis of a critical joint of a global model. Sometimes one sub-model might not be enough to get an accurate result, so the user can divide the sub-model again into an infinite number of parts as displacements should transfer from the global model to the sub-models. ANSYS software is more advanced for the sub-modelling technique. The folder of a sub-model is created automatically immediately after connecting the solution of the global model to the sub-model setup, which allows cut boundary constraints and displacement transfer from the global model to the sub-model. Fig. 3 shows the equivalent von Mises stress distribution through the thickness of the sub-models. Stress distribution might vary from sub-model to sub-model. Stresses can be measured by using the construction geometry path or surface, which would be created, based on a global coordinate system, as the global coordinate system should be the same for every sub-models. Therefore, the sub-models can be created only by duplicating the global model, and the sub-modelling technique might not work for other external domains.
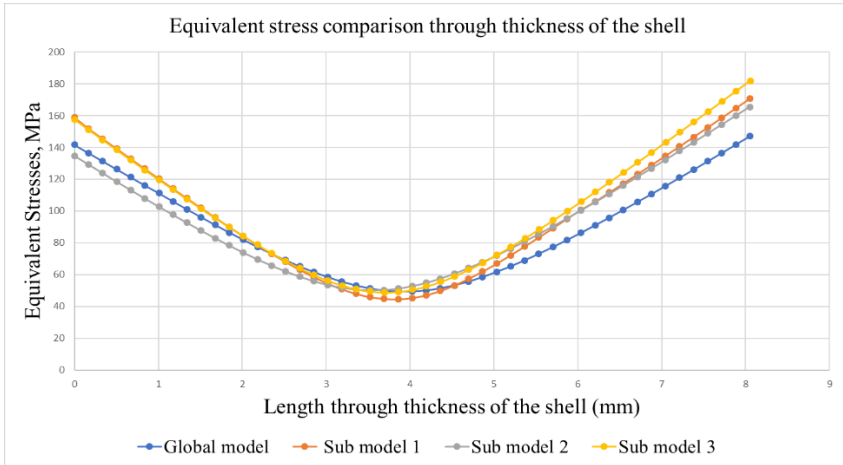

Fig. 3 Equivalent von Mises stress distribution through the thickness of the shell for global model and sub-models

Fig. 4 shows that the deformations are constant for every sub-model through the thickness of the shell (8 mm) calculated from ASME Section VIII Division 1, which confirmed that the nodal displacement transferred successfully from the global model to the sub-models.
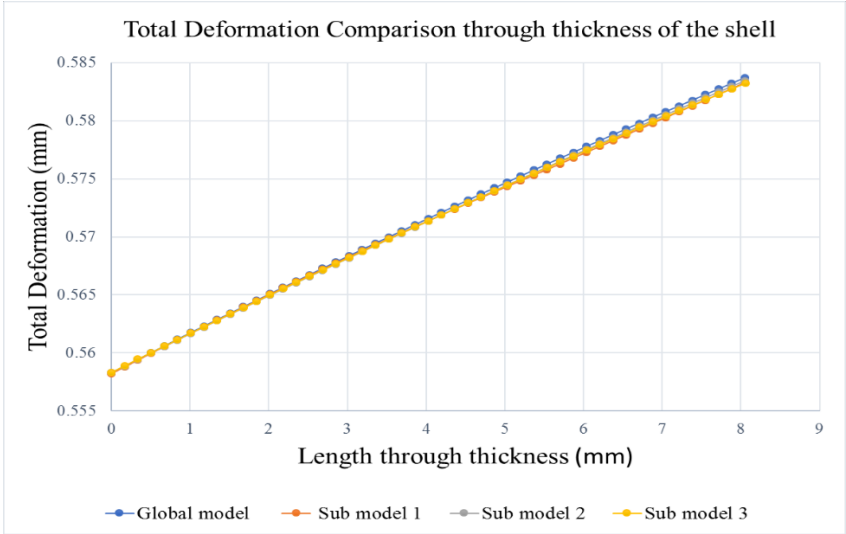
5

Fig. 4 Total deformation through the thickness of the shell.

One of the main goals of the sub-modelling technique is to achieve a fine mesh of the domain, which includes the region of interest. The comparison of course and fine mesh refinement is shown in Fig. 5, which shows the stress concentration is more at the weld toe region and the probability of crack initiation higher at this location. Equivalent stresses are increasing with mesh refinement, Coarse mesh gives a faster solution, but less accurate result; however, fine mesh gives a more precise result and need more time for calculation. Deformation would not affect the influence of mesh size, which remains the same along the weld toe region of the sub-model, which is shown in Fig. 6.
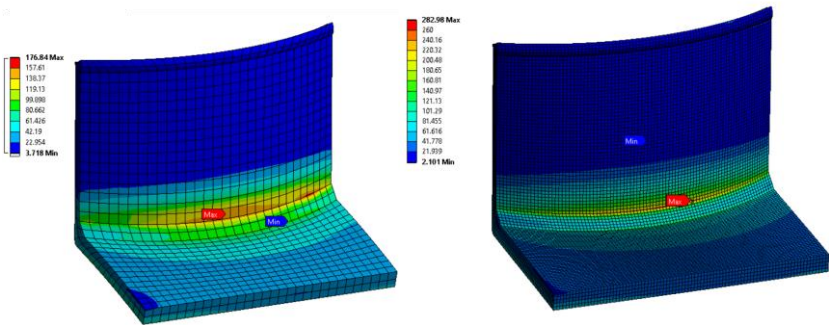

Fig. 5 Equivalent stress comparison for coarse and fine mesh of Sub-model 3
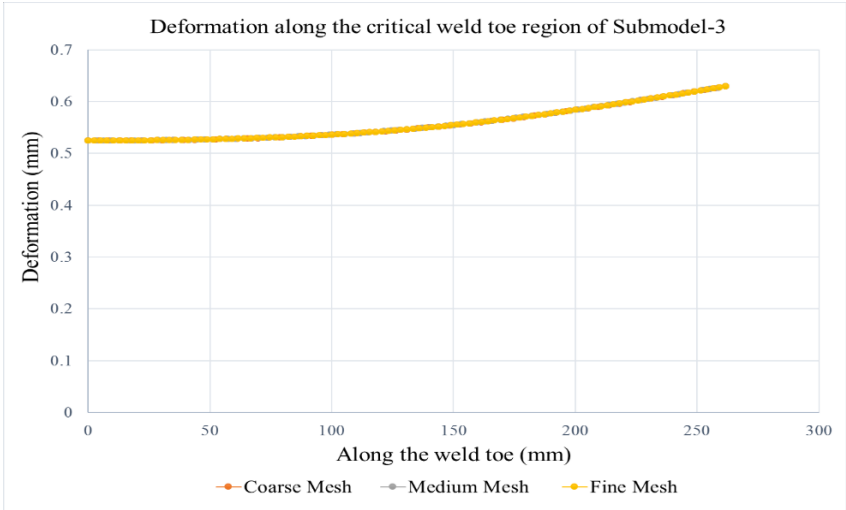
Fig. 6 Deformation along critical weld toe region

The stress concentration is higher at the weld toe region. By effective notch stress method, the stresses are calculated at the notches assumed to have linear elastic material characteristics.

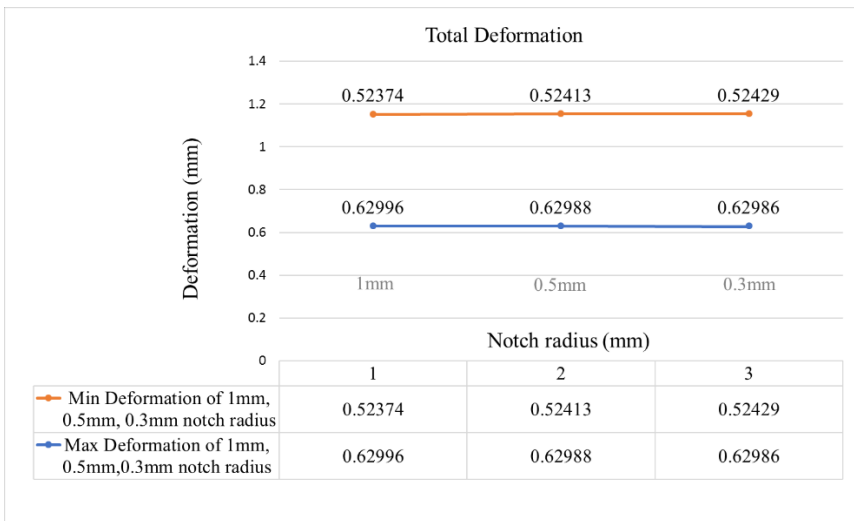|	Notch radius (mm)		
	1	2	3
Min Deformation of 1mm, 0.5mm, 0.3mm notch radius	0.52374	0.52413	0.52429
Max Deformation of 1mm, 0.5mm,0.3mm notch radius	0.62996	0.62988	0.62986

Fig. 7 Maximum and minimum deformations along the weld toe region of the sub-model 3, at different notch radius (1mm, 0.5mm, and 0.3mm).

7

Interpreting variation of weld shape parameters, as well as non-linear material behaviour at the notch root, the actual weld outline based on international design codes and standards, are replaced with an effective one. For structural steels, notch effective root radius of r = 1 mm has been given consistent results. At weld toes, effective notch stress assumed as at least 1.6 times as structural hot spot stress. [10]. The effective notch stress method is limited to the thickness **t** greater than or equal to 5 mm. Equivalent stresses and stress concentration would increase with respect notch radius. However, the measured deformations along the weld toe region at different notch radius are constant, which is shown in Fig.7, and the deformations are independent of notch radius. Therefore, the sub-modelling technique is valid for effective notch stress, crack prediction, and fracture mechanics calculations of complex welded structures.

4. Conclusion

Finite element analysis of a surge tank welded structure is reviewed with the sub-modelling technique, which is an effective and powerful method for fracture mechanics calculation, fatigue assessment, and non-linear study. Sub-modelling techniques give accurate results of critical parts of a complex structure, which would be applicable for marine structures, steel bridges, aerospace vehicles, wind turbines, etc. When comparing the results of sub-models, it was found that stresses are varying, however, the deformations are constant for several sub-models along the surface and through-thickness of the shell, which is independent of meshing and notch radius. Therefore, the interpolation of nodal displacements from the global model to the sub-models is accurate. However, a negligible error is occurring from one sub-model to another with a maximum of 0.1%.

References

1. **Narvydas, E.; Puodziuniene, N**. 2014. Applications of Sub-modeling in Structural Mechanics. Proceedings of 19th International Conference Mechanika 2014, Kaunas, Lithuania. 172–176.
2. Abaqus 2016 Analysis User's Guide. 2015. v. II: Analysis, Dassault Systèmes, 1529.
3. **Looman, A.D.** 2007. Submodeling in ANSYS Workbench, ANSYS Advantage 1(2): 34 – 36.
4. SOLIDWORKS Simulation. 2018. Online Help System. Dassault Systèmes, SolidWorks Corporation.
5. **Albuquerque, C.; Silva, A.L.L.; de Jesus, A.M.P., Calçada R.** 2015. An efficient methodology for fatigue damage assessment of bridge details using modal superposition of stress intensity factors, International Journal of Fatigue 81: 61-77.

http://dx.doi.org/10.1016/j.ijfatigue.2015.07.002

6. **Zhang, Y.M.; Yi, D.K.; Xiao, Z.M.; Huang Z.H.** 2015. Engineering critical assessment for offshore pipelines with 3-D elliptical embedded crack, Engineering Failure Analysis 51: 37-54.
   http://dx.doi.org/10.1016/j.engfailanal.2015.02.018

7. **Aristovich, K.Y.; Khan, S.H.** 2010. A new submodeling technique for multi-scale finite element computation of electromagnetic fields: Application in bioelectromagnetism, Journal of Physics: Conference Series 238: 1-8.
   http://dx.doi.org/10.1088/1742-6596/238/1/012050

8. **González-Albuixech, V.F.; Qian, G.; Sharabi, M.; Niffenegger, M.; Niceno, B.; Lafferty, N.** 2015. Comparison of PTS analyses of RPVs based on 3D- CFD and RELAP5, Nuclear Engineering and Design 291: 168-178.
   http://dx.doi.org/10.1016/j.nucengdes.2015.05.025

9. ASME Boiler and Pressure Vessel Code. 2017. Section VIII, Division 1, 2.

10. **Hobbacher, A. F.** 2016. Recommendations for Fatigue Design of Welded Joints and Components, 2nd edition. Springer International Publishing. XVI, 143 p.
    https://doi.org/10.1007/978-3-319-23757-2.

Abdul Khan THORAPPA, Evaldas NARVYDAS

Application of Sub-modelling Technique in Surge Tank Welded Structure

S u m m a r y

Stress analysis of surge tank welded structure using Sub-modelling techniques in finite element analysis are reviewed. Application of the sub-modelling technique is discussed with different softwares that are suitable for the model reduction technique. Compared the results of several segments of the sub-model and studied the behaviour of sub-models with mesh refinement, different notch radius, and thickness of the shell at the critical region of the structure.

Keywords: sub-modelling, finite element analysis, model reduction techniques, weld toe, stress concentration.